



THE UNIVERSITY *of* EDINBURGH

Edinburgh Research Explorer

## OSCILLATIONS IN A CAMP SIGNALING MODEL FOR CELL AGGREGATION { A GEOMETRIC ANALYSIS

### Citation for published version:

Miao, Z, Popovic, N & Szmolyan, P 2020, 'OSCILLATIONS IN A CAMP SIGNALING MODEL FOR CELL AGGREGATION { A GEOMETRIC ANALYSIS', *Journal of mathematical analysis and applications*, vol. 483, no. 1. <https://doi.org/10.1016/j.jmaa.2019.123577>

### Digital Object Identifier (DOI):

[10.1016/j.jmaa.2019.123577](https://doi.org/10.1016/j.jmaa.2019.123577)

### Link:

[Link to publication record in Edinburgh Research Explorer](#)

### Document Version:

Peer reviewed version

### Published In:

Journal of mathematical analysis and applications

### General rights

Copyright for the publications made accessible via the Edinburgh Research Explorer is retained by the author(s) and / or other copyright owners and it is a condition of accessing these publications that users recognise and abide by the legal requirements associated with these rights.

### Take down policy

The University of Edinburgh has made every reasonable effort to ensure that Edinburgh Research Explorer content complies with UK legislation. If you believe that the public display of this file breaches copyright please contact [openaccess@ed.ac.uk](mailto:openaccess@ed.ac.uk) providing details, and we will remove access to the work immediately and investigate your claim.



# OSCILLATIONS IN A cAMP SIGNALING MODEL FOR CELL AGGREGATION – A GEOMETRIC ANALYSIS

ZHOUQIAN MIAO, NIKOLA POPOVIĆ AND PETER SZMOLYAN

**ABSTRACT.** We study a singularly perturbed model for a cyclic adenosine monophosphate (cAMP) signaling system that controls aggregation of the amoeboid microorganism *Dictyostelium discoideum*. The model, which is based on a classical model due to Martiel and Goldbeter [16], takes the form of a planar system of ordinary differential equations with two singular perturbation parameters which manifest very differently: while one parameter encodes the separation of scales between the slow and fast variables, the other induces a non-uniformity in the corresponding vector field in the singular limit. We apply geometric singular perturbation theory and the desingularisation technique known as “blow-up” to construct a family of attracting, periodic (relaxation-type) orbits; in the process, we elucidate the novel singular structure of the model, and we describe in detail the resulting oscillatory dynamics.

## 1. INTRODUCTION

In the present article, we perform a geometric analysis of a singularly perturbed model for a cyclic adenosine monophosphate (cAMP) signaling system that controls aggregation of the amoeboid microorganism *Dictyostelium discoideum*. The periodic synthesis of pulses of cAMP constitutes an example of a biochemical oscillation of clear physiological significance [8]. Two main types of dynamics are observed in cAMP signaling systems: autonomous oscillation [5, 7, 8] and relay of super-threshold pulses [19, 22]. The model of cAMP signaling due to Goldbeter and Segel [9, 10] shows that both types are caused by the auto-catalytic regulation of adenylate cyclase, the latter enzyme being activated on the binding of extracellular cAMP to the cell receptor [6, 18]. Moreover, relay behaviour has been linked to autonomous oscillation, which represents the excitability of the system. In the model by Goldbeter and Segel, the substrate adenosine triphosphate (ATP) plays a role in the oscillation and relay response; however, it has been shown experimentally that intracellular ATP remains constant during the oscillation [20], and that the relay results from the absence of ATP consumption when the cAMP receptor is uncoupled from adenylate cyclase upon incubation with caffeine [24]. These observations were made under the assumption that adenylate cyclase is an allosteric enzyme; moreover, significant variation is required in the concentration of ATP. Martiel and Goldbeter [16] considered another situation, whereby the mechanism is based on desensitisation of the cAMP receptor to extracellular cAMP. The full model proposed in [16], which consists of seven differential equations, can be reduced to the three-variable system

$$\begin{aligned} (1a) \quad & \frac{d\rho_T}{dt} = -f_1(\gamma)\rho_T - f_2(\gamma)(1 - \rho_T), \\ (1b) \quad & \frac{d\beta}{dt} = q\sigma\phi(\rho_T, \gamma) - (k_i + k_t)\beta, \\ (1c) \quad & \frac{d\gamma}{dt} = \frac{k_t}{h}\beta - k_e\gamma, \end{aligned}$$

---

*Date:* October 10, 2019.

*Key words and phrases.* cAMP signaling; singular perturbation; geometric singular perturbation theory; blow-up technique; relaxation oscillation; periodic orbit.

with

$$(2a) \quad f_1(\gamma) = \frac{k_1 + k_2\gamma}{1 + \gamma}, \quad f_2(\gamma) = \frac{k_1L_1 + k_2L_2\gamma}{1 + c\gamma},$$

$$(2b) \quad \phi(\rho_T, \gamma) = \frac{\alpha(\lambda\theta + \epsilon Y^2)}{1 + \alpha\theta + \epsilon Y^2(1 + \alpha)}, \quad \text{and} \quad Y = \frac{\rho_T\gamma}{1 + \gamma}.$$

Here,  $\rho_T$  represents the total fraction of receptor in the active state, while  $\beta$  and  $\gamma$  denote intracellular and extracellular concentrations, respectively, of cAMP. Moreover,  $c, \alpha, \lambda, \theta, \epsilon, \sigma, h, k_i, k_t, k_e, k_j, L_j$  ( $j = 1, 2$ ), and  $q$  are suitably defined parameters; details can be found in [16]. Equation (1) can be reduced further to a two-variable system for sufficiently large values of the parameters  $q, k_i$ , and  $k_t$ , which allows for a quasi-steady-state assumption to be made for  $\beta$ : Equation (1b) implies  $\beta = q\sigma \frac{\phi(\rho_T, \gamma)}{(k_i + k_t)}$ . Therefore, the effective dynamics is then characterised by the following planar system of nonlinear ordinary differential equations (ODEs),

$$(3a) \quad \frac{d\rho_T}{dt} = -f_1(\gamma)\rho_T - f_2(\gamma)(1 - \rho_T),$$

$$(3b) \quad \frac{d\gamma}{dt} = \frac{q\sigma k_t}{h(k_i + k_t)}\phi(\rho_T, \gamma) - k_e\gamma.$$

While experiments [16] indicate that  $q \gg 1$ , whereas  $k_i$  and  $k_t$  are of the order  $\mathcal{O}(1)$ , and hence lower than what is expected for a quasi-steady-state assumption, numerical simulation shows that the planar system in (3) provides a reasonably good approximation for the three-variable system in (1). Therefore, (3) can be considered as the core mechanism in the cAMP signaling system, allowing for a phase plane analysis for relay and oscillation due to the simplicity of the governing equations.

With these observations in mind, we now introduce the singular perturbation problem considered in the present article, which is based on the three-variable Martiel-Goldbeter model, Equation (1), in the scaling of Liţcanu and Velázquez [15]:

$$(4a) \quad R_\tau = \kappa(U + \mathcal{P}\varepsilon) \left[ \frac{\mu(U + \varepsilon) - (U + d\varepsilon)R}{(U + \frac{\varepsilon}{c})(U + \varepsilon)} \right],$$

$$(4b) \quad W_\tau = \frac{b\varepsilon(U + \varepsilon)^2 + \Theta R^2 U^2}{(U + \varepsilon)^2 + \Lambda R^2 U^2} - W,$$

$$(4c) \quad U_\tau = \Gamma(W - U).$$

The state variables, which are now denoted by  $R, W$ , and  $U$ , correspond to the total proportion of receptors in the active state  $\rho_T$ , the concentration of intracellular cAMP  $\beta$ , and the concentration of extracellular cAMP  $\gamma$ , respectively; the model parameters are defined in Table 1, with  $\tau = (k_i + k_t)t$ .

Imposing a quasi-steady-state assumption, as was done for (1) above, we find  $W = U$ , thus reducing the model to the two-variable system

$$(5a) \quad R_\tau = \kappa(U + \mathcal{P}\varepsilon) \frac{\mu(U + \varepsilon) - (U + d\varepsilon)R}{(U + \frac{\varepsilon}{c})(U + \varepsilon)},$$

$$(5b) \quad U_\tau = \frac{b\varepsilon(U + \varepsilon)^2 + \Theta R^2 U^2}{(U + \varepsilon)^2 + \Lambda R^2 U^2} - U.$$

Given the definition of the parameters  $\kappa$  and  $\varepsilon$  in [15], which are both assumed to be small, (5) is singularly perturbed (“slow-fast”). Here, we emphasise that the impact of these two parameters on the dynamics of (5) manifests very differently: while the parameter  $\kappa$  is a “conventional” singular perturbation parameter that reflects the separation of scales between the slow variable  $R$  and the fast variable  $U$ , the parameter  $\varepsilon$  induces a different type of singular perturbation which is reflected by the non-uniformity of the limit as  $\varepsilon \rightarrow 0$  in Equation (5); specifically, that limit will depend fundamentally on whether  $U \gg \varepsilon$  or  $U = \mathcal{O}(\varepsilon)$  therein. Correspondingly, the limit as  $\kappa \rightarrow 0$  in Equation (5) can be studied using Fenichel’s geometric singular perturbation

theory [4], while the structure of the resulting asymptotics in  $\varepsilon$  can be resolved rigorously via the blow-up technique [3]. In particular, geometric singular perturbation theory implies that normally hyperbolic portions of the so-called critical manifold, which is obtained for  $\kappa = 0$  in (5), persist for  $\kappa$  positive and sufficiently small. However, since the geometry of that critical manifold degenerates in the limit as  $\varepsilon \rightarrow 0$ , a blow-up analysis in  $\varepsilon$  is performed to remove that degeneracy.

While our article is self-contained, we expect some familiarity on the part of the reader with geometric singular perturbation theory and the blow-up technique; see again [3, 11, 12, 14] for details. For an introduction in the context of the present family of problems, the reader is referred to Appendix A of [13].

**Remark 1.** Since Equation (4c) can be written as  $\frac{1}{\Gamma}U_\tau = (W - U)$ , and since  $\frac{\partial}{\partial U}(W - U) = -1$ , the above quasi-steady-state assumption can be interpreted geometrically [4] as a global reduction to the critical manifold  $\{W = U\}$ , with singular perturbation parameter  $\Gamma^{-1}$ . For the value of  $\Gamma$  given in Table 1, that reduction is not justified, strictly speaking; however, we follow the biologically motivated reasoning in [9] here.

Our analysis of Equation (5) has some similarities to the study of the Goldbeter-Lefever model [21] in [13]; there, the critical manifold was found to consist of two non-hyperbolic lines and one normally hyperbolic line. The blow-up technique was then applied to achieve a complete desingularisation of the flow near that manifold, whereby the non-hyperbolic lines were blown up to intersecting cylinders, allowing the authors to prove the occurrence of relaxation oscillation in the system.

While Equation (5) shares some characteristics of the Goldbeter-Lefever model studied in [13], it is slightly more degenerate: as will turn out, the critical manifold here is the union of one non-hyperbolic line in the “inner” region and one normally hyperbolic curve in the “outer” region, which meet in a degenerate steady state at the origin. Moreover, the  $U$ -variable has to be scaled with the singular parameter  $\varepsilon$  due to the presence of the term  $(U + \varepsilon)^2 + \Lambda R^2 U^2$  in (5b), as  $\varepsilon$  cannot be eliminated by a simple change of coordinates, which represents the major conceptual difference to the model considered in [13]. Therefore, the resulting singularly perturbed structure is novel; our resolution of that structure, and in particular of the highly degenerate flow near the origin in  $(R, U, \varepsilon)$ -space, results in improved understanding of the oscillatory dynamics that is observed in the reformulated singular perturbation problem of cAMP signaling, Equation (5).

In accordance with the numerical values given in Table 1, we rescale the parameters  $\mu = \tilde{\mu}\varepsilon^{\frac{1}{2}}$ ,  $d = \tilde{d}\varepsilon^{\frac{1}{2}}$ , and  $b = \tilde{b}\varepsilon$  in (5). These scalings broadly agree with assumptions made in [15], where it was postulated that  $\mu \sim d$ ,  $\mu \simeq \varepsilon$ , and  $b \ll 1$ ; however, we rescale  $\mu$  and  $d$  with  $\varepsilon^{\frac{1}{2}}$  instead of with  $\varepsilon$  here, which is consistent with the basic geometry of oscillation found in [16] for the three-dimensional system, Equation (1). Moreover, we rewrite the resulting equations in the equivalent form

$$(6a) \quad R' = \kappa(U + \mathcal{P}\varepsilon) \frac{(U + \varepsilon)^2 + \Lambda R^2 U^2}{(U + \varepsilon)(U + \frac{\varepsilon}{c})} [\tilde{\mu}\varepsilon^{\frac{1}{2}}(U + \varepsilon) - (U + \tilde{d}\varepsilon^{\frac{3}{2}})R],$$

$$(6b) \quad U' = \tilde{b}\varepsilon^2(U + \varepsilon)^2 + \Theta R^2 U^2 - U[(U + \varepsilon)^2 + \Lambda R^2 U^2],$$

which is obtained by formally multiplying the right-hand sides in (5) with a (polynomial) factor of  $(U + \varepsilon)^2 + \Lambda R^2 U^2$ . (Since that factor is non-negative, the corresponding transformation of time does not change the direction of the flow.) Here, the prime now denotes differentiation with respect to the new, rescaled time.

**Remark 2.** The apparent singularity of Equation (6) at  $(U, \varepsilon) = (0, 0)$  will be resolved by blow-up; in fact, the right-hand side in (6a) vanishes to at least second order in  $(U, \varepsilon)$ , which implies  $\mathcal{C}^2$ -smoothness of the corresponding vector field in both  $U$  and  $\varepsilon$ .

The following is the main result of our analysis:

TABLE 1. Definition and numerical values, with orders of magnitude, of the parameters in (59); cf. [15], where the quantities in the second column are defined.

Parameter	Definition	Order of magnitude	Numerical value
$\kappa$	$\frac{k_2(1+L_2)}{k_i+k_t}$	$\ll 1$	0.0023
$\mu$	$\frac{m+d}{m+1}$	$\ll 1 \sim d$	0.1274
$\varepsilon$	$M^{-1}$	$\ll 1$	0.1258
$d$	$\frac{1+L_1}{c+L_1}$	$\ll 1$	0.1
$b$	$\frac{\alpha q \sigma k_t}{(k_i+k_t)h} \frac{\lambda \theta}{1+\alpha \theta}$	$\ll 1$	0.01587
$\Gamma$	$\frac{k_e}{k_i+k_t}$	$\simeq 1$	2.1052
$\Lambda$	$(A\mu^2)^{-1}$	$\simeq 1$	0.2966
$\Theta$	$\Lambda B \varepsilon$	$\simeq 1$ or $\gg 1$	1.5087
$c$		$\gg 1$	100
$\mathcal{P}$	$\frac{k_1}{k_2}$	$\gg 1$	100

**Theorem 1.** *Let  $\varepsilon \in (0, \varepsilon_0]$ , with  $\varepsilon_0$  positive and sufficiently small. Then, there exists  $\kappa_0 = \kappa_0(\varepsilon_0)$  such that, for  $\kappa \in (0, \kappa_0]$ , Equation (6) admits a unique family of attracting periodic orbits  $\Gamma_{\kappa\varepsilon}$  which tends to a singular cycle  $\Gamma_{0\varepsilon}$  as  $\kappa \rightarrow 0$  uniformly for  $\varepsilon \in (0, \varepsilon_0]$ , and to a singular cycle  $\Gamma_{00}$  as  $(\kappa, \varepsilon) \rightarrow (0, 0)$ .*

**Remark 3.** We emphasise that  $\Gamma_{0\varepsilon}$  and  $\Gamma_{00}$  are defined implicitly, i.e., via  $\Gamma_{\kappa\varepsilon}$ , in the statement of Theorem 1; an explicit definition will be provided through the following analysis.

A visualisation of the assertions made in Theorem 1 can be found in Figure 1, where the nullclines of Equation (6) are sketched in addition to the singular cycles  $\Gamma_{00}$  and  $\Gamma_{0\varepsilon}$ , as well as a sample periodic orbit  $\Gamma_{\kappa\varepsilon}$  which was obtained numerically. Here, the values of the relevant parameters are as specified in Table 1, with the exception of  $\kappa(= 0.00023)$ ,  $\mu(= 0.13)$ , and  $d(= 0.071)$ ; the latter two are chosen such that the unique equilibrium in the system is shifted to the middle branch of the  $U$ -nullcline, thus allowing for excitability and, hence, oscillatory dynamics.

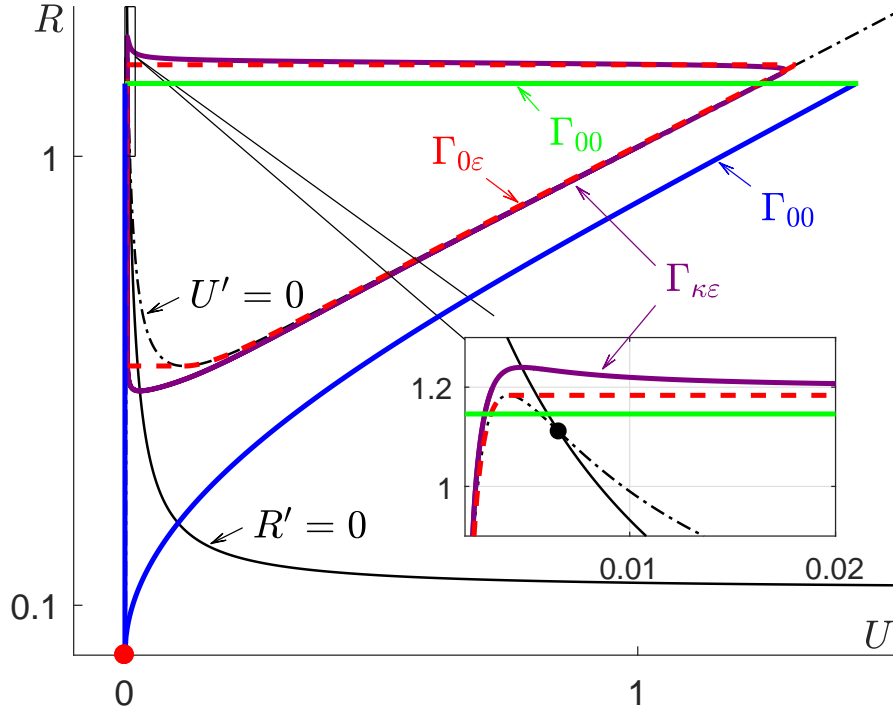


FIGURE 1. Nullclines and periodic orbits for Equation (6), with parameter values as in Table 1:  $R$ -nullcline (solid black);  $U$ -nullcline (dash-dotted black); singular cycle  $\Gamma_{00}$  (solid blue; solid green); singular cycle  $\Gamma_{0\varepsilon}$  (dashed red); periodic orbit  $\Gamma_{\kappa\varepsilon}$  (solid purple); equilibrium (inset).

In the remainder of the article, we will prove Theorem 1 by constructing a family of periodic (relaxation-type) cycles for Equation (6); as is common in singular perturbation theory, we will first identify a singular orbit when  $\kappa = 0 = \varepsilon$ . Subsequently, we will show the persistence of that orbit for  $\kappa$  and  $\varepsilon$  positive, but small. Our analysis follows that of Kosiuk and Szmolyan [13] in spirit, subject to the appropriate modifications due to differences in the singular structure of (6); in particular, our focus is on the resulting asymptotics in  $\varepsilon$ , which is discussed in detail, whereas the relatively standard perturbation analysis with respect to  $\kappa$  is treated in a more cursory fashion.

## 2. SINGULAR DYNAMICS

As Equation (6) for  $\varepsilon > 0$  represents a slow-fast system in standard form, with singular perturbation parameter  $\kappa$ , we rewrite the corresponding flow on the slow time-scale to obtain the equivalent formulation

$$(7a) \quad \dot{R} = (U + \mathcal{P}\varepsilon) \frac{(U + \varepsilon)^2 + \Lambda R^2 U^2}{(U + \varepsilon)(U + \frac{\varepsilon}{c})} [\tilde{\mu}\varepsilon^{\frac{1}{2}}(U + \varepsilon) - (U + \tilde{d}\varepsilon^{\frac{3}{2}})R],$$

$$(7b) \quad \kappa \dot{U} = \tilde{b}\varepsilon^2(U + \varepsilon)^2 + \Theta R^2 U^2 - U[(U + \varepsilon)^2 + \Lambda R^2 U^2].$$

In our analysis, we hence first consider the singular limit of  $\kappa = 0$  in Equations (6) and (7). The small- $\varepsilon$  dynamics in that limit will be studied separately in different scaling regimes  $\mathcal{R}_j$  ( $j = 1, 2, 3$ ), which are defined in Section 3 below.

2.1. **Slow-fast analysis for  $\kappa = 0$  and  $\varepsilon > 0$ .** Setting  $\kappa = 0$  in Equations (6) and (7) for fixed, positive  $\varepsilon$  defines two limiting systems, the “layer problem”

$$(8a) \quad R' = 0,$$

$$(8b) \quad U' = \tilde{b}\varepsilon^2(U + \varepsilon)^2 + \Theta R^2 U^2 - U[(U + \varepsilon)^2 + \Lambda R^2 U^2]$$

and the “reduced problem”

$$(9a) \quad \dot{R} = (U + \mathcal{P}\varepsilon) \frac{(U + \varepsilon)^2 + \Lambda R^2 U^2}{(U + \varepsilon)(U + \frac{\varepsilon}{c})} [\tilde{\mu}\varepsilon^{\frac{1}{2}}(U + \varepsilon) - (U + \tilde{d}\varepsilon^{\frac{3}{2}})R],$$

$$(9b) \quad 0 = \tilde{b}\varepsilon^2(U + \varepsilon)^2 + \Theta R^2 U^2 - U[(U + \varepsilon)^2 + \Lambda R^2 U^2].$$

The critical manifold  $\mathcal{S}_{0\varepsilon}$ , which is defined by (9b), is precisely the  $U$ -nullcline in Equation (6). The manifold  $\mathcal{S}_{0\varepsilon}$  is  $S$ -shaped; linearisation of the layer problem, Equation (8), about  $\mathcal{S}_{0\varepsilon}$  shows that  $\frac{\partial}{\partial U} \{ \tilde{b}\varepsilon^2(U + \varepsilon)^2 + \Theta R^2 U^2 - U[(U + \varepsilon)^2 + \Lambda R^2 U^2] \}$  has zeroes at  $U_{0\varepsilon}^A = 2\tilde{b}\varepsilon^2 + \mathcal{O}(\varepsilon^3)$  and  $U_{0\varepsilon}^C = \varepsilon + \mathcal{O}(\varepsilon^2)$ . Hence,  $\mathcal{S}_{0\varepsilon}$  consists of three branches, which are separated by two fold points at  $A_{0\varepsilon} : (R_{0\varepsilon}^A, U_{0\varepsilon}^A)$  and  $C_{0\varepsilon} : (R_{0\varepsilon}^C, U_{0\varepsilon}^C)$ , with  $R_{0\varepsilon}^A = \frac{1}{2\sqrt{\Theta\tilde{b}}} + \mathcal{O}(\varepsilon)$  and  $R_{0\varepsilon}^C = \frac{2}{\sqrt{\Theta}}\varepsilon^{\frac{1}{2}} + \mathcal{O}(\varepsilon)$ ; the left branch  $\mathcal{S}_{0\varepsilon}^{a-}$  and the right branch  $\mathcal{S}_{0\varepsilon}^{a+}$  are attracting under the layer flow of Equation (6), while the middle branch  $\mathcal{S}_{0\varepsilon}^r$  is repelling.

**Remark 4.** For  $\varepsilon$  non-small in the statement of Theorem 1, Equation (6) admits standard relaxation-type cycles [23] for  $\kappa \in (0, \kappa_0]$  sufficiently small, with  $\kappa_0 = \kappa_0(\varepsilon)$ , as long as the critical manifold  $\mathcal{S}_{0\varepsilon}$  remains  $S$ -shaped; in fact, for the parameter values given in Table 1, that is the case for  $\varepsilon$  up to the order of 10. However, our focus here is on  $\varepsilon$  small, due to the degenerate singular structure of  $\mathcal{S}_{0\varepsilon}$  as  $\varepsilon \rightarrow 0$ ; see Section 2.2 below.

We denote the unique equilibrium of (6), which is found in the intersection of the  $R$ -nullcline with  $\mathcal{S}_{0\varepsilon}$ , by  $E_{0\varepsilon}$ ; see Figure 2. (Due to our assumptions on the parameters  $d$ ,  $\mu$ , and  $\Theta$ ,  $E_{0\varepsilon}$  is, in fact, located on the middle branch  $\mathcal{S}_{0\varepsilon}^r$  of  $\mathcal{S}_{0\varepsilon}$ .) Analysis of the reduced flow on  $\mathcal{S}_{0\varepsilon}$  shows that  $R$  increases below the point  $A_{0\varepsilon}$  on  $\mathcal{S}_{0\varepsilon}^{a-}$ , while it decreases on  $\mathcal{S}_{0\varepsilon}^{a+}$ . (The direction of the flow on  $\mathcal{S}_{0\varepsilon}^r$ , as indicated in Figure 2, is determined by the sign of the term  $[\tilde{\mu}\varepsilon^{\frac{1}{2}}(U + \varepsilon) - (U + \tilde{d}\varepsilon^{\frac{3}{2}})R]$  in (9a).) Hence, we obtain the following standard singular relaxation-type dynamics for  $\kappa = 0$  and fixed, positive  $\varepsilon$ : orbits starting on  $\mathcal{S}_{0\varepsilon}^{a-}$  jump at the fold point  $A_{0\varepsilon}$  and reach a point  $D_{0\varepsilon}$  on  $\mathcal{S}_{0\varepsilon}^{a+}$  along the 1-dimensional stable manifold thereof; they then follow the reduced dynamics on  $\mathcal{S}_{0\varepsilon}^{a+}$  until they reach the fold point at  $C_{0\varepsilon}$ , from where they jump back to a point  $B_{0\varepsilon}$  on  $\mathcal{S}_{0\varepsilon}^{a-}$  along the 1-dimensional stable manifold thereof; finally, they follow the reduced dynamics on  $\mathcal{S}_{0\varepsilon}^{a-}$  until they reach  $A_{0\varepsilon}$ , at which point the above dynamics repeats. Correspondingly, we define the singular cycle  $\Gamma_{0\varepsilon}$ , which consists of the heteroclinic orbit  $\Gamma_{0\varepsilon}^{AD}$  connecting  $A_{0\varepsilon}$  to  $D_{0\varepsilon}$  under the layer flow of (8), the segment  $\Gamma_{0\varepsilon}^{DC}$  of  $\mathcal{S}_{0\varepsilon}^{a+}$  from  $D_{0\varepsilon}$  to  $C_{0\varepsilon}$ , the heteroclinic orbit  $\Gamma_{0\varepsilon}^{CB}$  connecting  $C_{0\varepsilon}$  to  $B_{0\varepsilon}$  under the layer flow, and the segment  $\Gamma_{0\varepsilon}^{BA}$  of  $\mathcal{S}_{0\varepsilon}^{a-}$  between  $B_{0\varepsilon}$  and  $A_{0\varepsilon}$ ; cf. again Figure 2.

**Remark 5.** Here and in the following, reduced dynamics is depicted in blue, while the corresponding layer flow is shown in green; double arrows indicate hyperbolicity, while non-hyperbolic dynamics is indicated with single arrows.

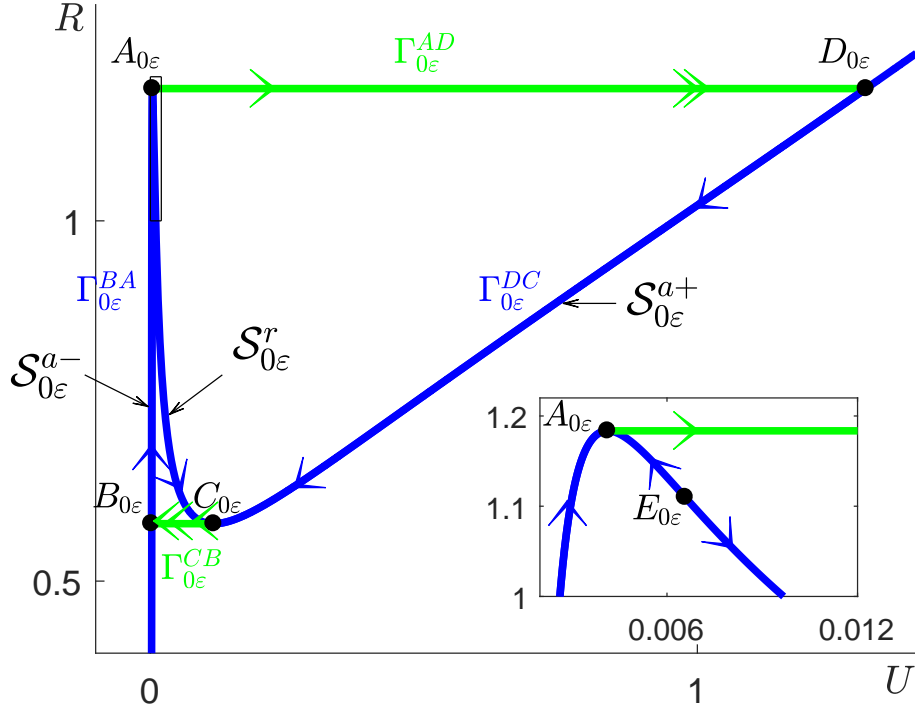


FIGURE 2. Reduced flow on the critical manifold  $\mathcal{S}_{0\epsilon}$  (solid blue), layer dynamics (solid green), singular cycle  $\Gamma_{0\epsilon}$  (solid blue; solid green), and equilibrium  $E_{0\epsilon}$  (inset) for Equation (8), with parameter values as in Table 1.

It follows from [14, Theorem 2.3] that  $\Gamma_{0\epsilon}$  persists, for  $\epsilon$  positive and fixed and  $\kappa$  sufficiently small, as an attracting relaxation-type cycle of Equation (6). However, as (6) constitutes a two-parameter singular perturbation problem, we are interested in the double limit as  $\kappa$  and  $\epsilon$  tend to zero simultaneously.

**2.2. Slow-fast analysis for  $\kappa = 0 = \epsilon$ .** As will turn out, the limit as  $(\kappa, \epsilon) \rightarrow (0, 0)$  in Equation (6) is significantly more singular than the limit of  $\kappa \rightarrow 0$  with  $\epsilon$  fixed, as considered in the previous subsection.

For  $(\kappa, \epsilon) = (0, 0)$ , (6) yields the seemingly simple layer problem

$$(10a) \quad R' = 0,$$

$$(10b) \quad U' = \Theta R^2 U^2 - U(U^2 + \Lambda R^2 U^2),$$

which corresponds precisely to the system that is obtained from (8) for  $\epsilon = 0$ . Equation (10) admits two sets of equilibria; one of these satisfies  $U = 0$ , while the other is defined by  $\Theta R^2 - (U + \Lambda R^2 U) = 0$ . Hence, the critical manifold  $\mathcal{S}_{00}$  for (10) consists of the curves  $\mathcal{S}_{00}^r = \{(R, 0) \mid R > 0\}$  and  $\mathcal{S}_{00}^{a+} = \{(R, U) \mid R > 0, U = \frac{\Theta R^2}{1 + \Lambda R^2}\}$ , which meet in the origin  $Q$ . (Clearly,  $\mathcal{S}_{00}$  coincides with the critical manifold  $\mathcal{S}_{0\epsilon}$  when  $\epsilon = 0$ .) Linearisation of Equation (10) about  $\mathcal{S}_{00}$  shows that the curve  $\mathcal{S}_{00}^{a+}$  is normally hyperbolic, while  $\mathcal{S}_{00}^r$  – the  $R$ -axis – and the point  $Q$  are non-hyperbolic; see Figure 3 for an illustration.



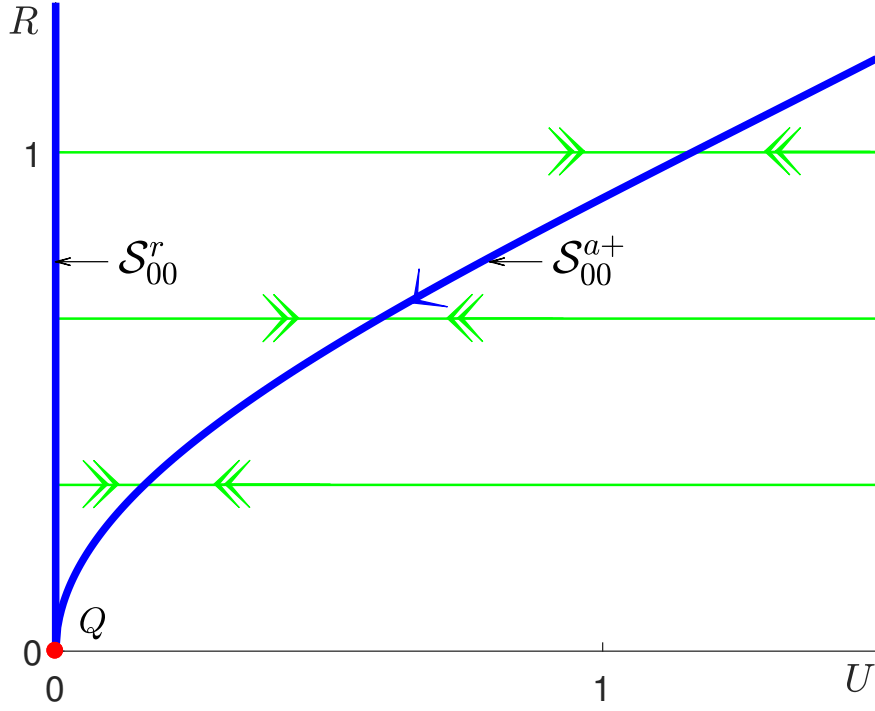


FIGURE 3. Reduced flow on the critical manifold  $\mathcal{S}_{00}$  (solid blue), layer dynamics (solid green), and non-hyperbolic origin  $Q$  (red dot) for Equation (10).

In particular, it follows that, for  $U$  and  $R$  bounded away from zero, the critical manifold  $\mathcal{S}_{0\varepsilon}^{a+}$  introduced in the previous subsection is a regular perturbation (in  $\varepsilon$ ) of the manifold  $\mathcal{S}_{00}^{a+}$  defined above. Hence, standard theory [4] can be applied to show the persistence of  $\mathcal{S}_{00}^{a+}$  for  $\kappa$  and  $\varepsilon$  positive and small in that case:

**Proposition 1.** *Let  $\varepsilon \in [0, \varepsilon_0]$  be fixed, and let  $\kappa \in [0, \kappa_0]$ , with  $\varepsilon_0$  and  $\kappa_0$  positive and sufficiently small. Moreover, let  $U \in [\underline{\alpha}, \bar{\alpha}]$  and  $R \in [\underline{\beta}, \bar{\beta}]$ , where  $\underline{\alpha}$  and  $\underline{\beta}$  are positive and small, but independent of  $(\kappa, \varepsilon)$ , and  $\bar{\alpha}$  and  $\bar{\beta}$  are assumed to be  $\mathcal{O}(1)$ . Then, the following statements hold:*

1. For  $\kappa = 0$ , Equation (8) admits the critical manifold

$$(11) \quad \mathcal{S}_{0\varepsilon}^{a+} = \{(R, U) \mid R \in [\underline{\beta}, \bar{\beta}], U = \Phi_{0\varepsilon}(R)\};$$

here, the function  $\Phi_{0\varepsilon}$  satisfies

$$\Phi_{0\varepsilon}(R) = \frac{\Theta R^2}{1 + \Lambda R^2} + \frac{\tilde{b}}{1 + \Lambda R^2} \varepsilon^2 + \mathcal{O}(\varepsilon^3).$$

2. The manifold  $\mathcal{S}_{0\varepsilon}^{a+}$  is normally attracting, with a single negative eigenvalue  $-\frac{\Theta^2 R^4}{1 + \Lambda R^2}$ .
3. The reduced flow on  $\mathcal{S}_{0\varepsilon}^{a+}$  is given by

$$\dot{R} = -\frac{\Theta^2 R^5}{1 + \Lambda R^2} + \frac{\Theta^2 R^4 \tilde{\mu}}{1 + \Lambda R^2} \sqrt{\varepsilon} + \mathcal{O}(\varepsilon),$$

which implies, in particular,  $\dot{R} < 0$  for  $\varepsilon$  sufficiently small.

4. For  $\kappa$  positive and small, the manifold  $\mathcal{S}_{0\varepsilon}^{a+}$  perturbs to a manifold

$$(12) \quad \mathcal{S}_{\kappa\varepsilon}^{a-} = \{(R, U) \mid R \in [\underline{\beta}, \bar{\beta}], U = \Phi_{\kappa\varepsilon}(R)\},$$

where  $\Phi_{\kappa\varepsilon} = \Phi_{0\varepsilon} + \mathcal{O}(\kappa)$  is regular in  $(\kappa, \varepsilon)$  to any order therein.

**Remark 6.** Comparison of Figures 2 and 3 shows that the manifolds  $\mathcal{S}_{0\varepsilon}^{a-}$  and  $\mathcal{S}_{0\varepsilon}^r$  merge into  $\mathcal{S}_{00}^r$  in the limit as  $\varepsilon \rightarrow 0$ ; correspondingly, the points  $B_{0\varepsilon}$  and  $C_{0\varepsilon}$  coalesce into the origin  $Q$  in that limit.

### 3. SCALING REGIMES

The discussion in Section 2 indicates that, for  $\varepsilon = 0$ , essential portions of the sought-after relaxation cycle  $\Gamma_{\kappa\varepsilon}$  for Equation (6) are “hidden” in the non-hyperbolic line  $\mathcal{S}_{00}^r$  and the point  $Q$ ; specifically, it is intuitively clear that  $\mathcal{S}_{0\varepsilon}^{a-}$  and  $\mathcal{S}_{0\varepsilon}^r$  merge into  $\mathcal{S}_{00}^r$  in that limit, while the fold point  $C_{0\varepsilon}$  converges to the origin  $Q$ . Appropriate rescalings of  $R$  and  $U$  are required in order to make these aspects of the dynamics visible in different scaling regimes. These regimes are denoted by  $\mathcal{R}_j$  ( $j = 1, 2, 3$ ), and are defined as follows:

- (1) Regime  $\mathcal{R}_1$ :  $U = \mathcal{O}(\varepsilon^2)$ ,  $R = \mathcal{O}(1)$ ;
- (2) Regime  $\mathcal{R}_2$ :  $U = \mathcal{O}(\varepsilon)$ ,  $R = \mathcal{O}(\varepsilon^{\frac{1}{2}})$ ;
- (3) Regime  $\mathcal{R}_3$ :  $U = \mathcal{O}(1)$ ,  $R = \mathcal{O}(1)$ .

In particular, the “inner” and “outer” regions, which are mentioned in the Introduction, are covered by regimes  $\mathcal{R}_j$  ( $j = 1, 2$ ) and regime  $\mathcal{R}_3$ , respectively; see Figure 4.

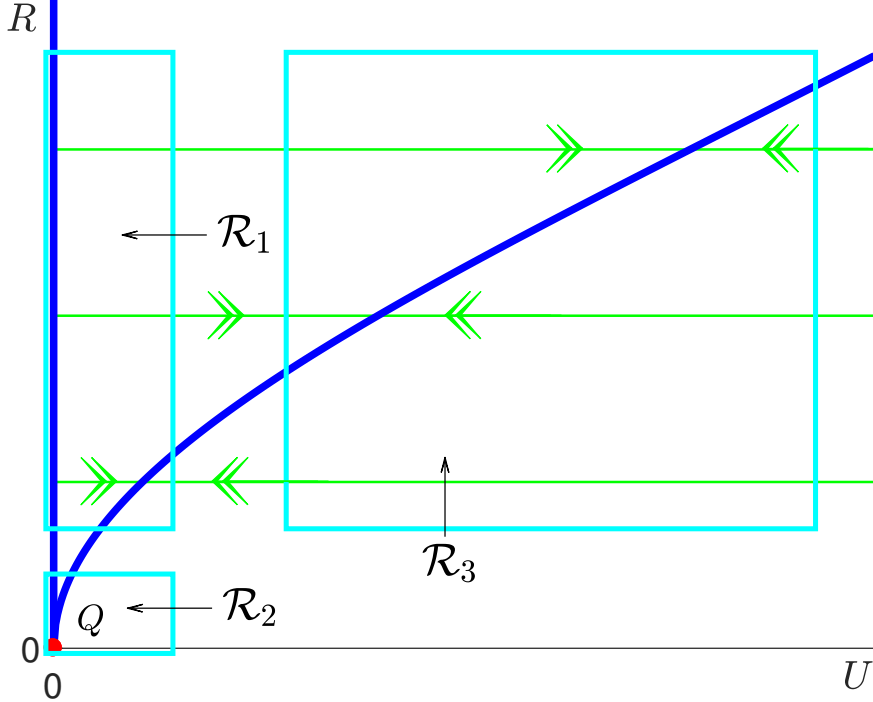


FIGURE 4. The scaling regimes  $\mathcal{R}_1$ ,  $\mathcal{R}_2$ , and  $\mathcal{R}_3$  for Equation (6).

The above scalings in  $U$  then also imply the corresponding scalings of  $R$ , and can be substantiated via the method of Newton polygons [2], which shows in particular that the parameter  $b$  must be of the order  $\mathcal{O}(\varepsilon)$ , as assumed above. Finally, the scalings in regimes  $\mathcal{R}_1$  and  $\mathcal{R}_2$  are consistent with the  $\varepsilon$ -dependence of the two fold points of Equation (6) at  $A_{0\varepsilon}$  and  $C_{0\varepsilon}$ , respectively – or, rather, of the  $(R, U)$ -coordinates thereof.

In this section, we will discuss the geometry in the three regimes  $\mathcal{R}_j$  ( $j = 1, 2, 3$ ) in turn to motivate how the “full” singular dynamics of Equation (6) can be desingularised to allow for a description of the resulting, global oscillation. Our discussion will be substantiated, and made fully rigorous, in subsequent sections, where a desingularisation will be achieved via the

blow-up technique. In particular, as the three regimes introduced above do not overlap, it is not *a priori* evident how to match them; here, we will show that matching can be accomplished in various coordinate charts – so-called “phase-directional charts” – after blow-up, as was also done in [13]. (We emphasise that these charts are not covered by the scaling regimes themselves, which correspond to “rescaling charts” in the blow-up, but that they arise naturally in our blow-up analysis.)

**3.1. Regime  $\mathcal{R}_1$ :**  $U = \mathcal{O}(\varepsilon^2)$ ,  $R = \mathcal{O}(1)$ . Regime  $\mathcal{R}_1$  covers a neighbourhood of the  $R$ -axis that is, however, bounded away from the origin  $Q$ . Correspondingly, we introduce the scaling

$$(13) \quad R = R_1 \quad \text{and} \quad U = \varepsilon^2 U_1$$

in that regime. For the sake of definiteness, we assume that  $U_1 \in [0, \bar{\alpha}_1]$  and  $R_1 \in [\beta_1, \bar{\beta}_1]$ , where  $\bar{\alpha}_1$  is assumed to be large,  $\beta_1$  is small, and  $\bar{\beta}_1$  is  $\mathcal{O}(1)$ , corresponding to our assumption that the original variables  $U$  and  $R$  satisfy  $U = \mathcal{O}(\varepsilon^2)$  and  $R = \mathcal{O}(1)$ ; see Figure 5.

After dividing out the factor  $\varepsilon^2$ , we obtain the following system of equations from Equation (6):

$$(14a) \quad R'_1 = \kappa \varepsilon^{\frac{1}{2}} (\varepsilon U_1 + \mathcal{P}) \frac{(\varepsilon U_1 + 1)^2 + \Lambda R_1^2 \varepsilon^2 U_1^2}{(\varepsilon U_1 + 1)(\varepsilon U_1 + \frac{1}{\varepsilon})} [\tilde{\mu}(\varepsilon U_1 + 1) - (\varepsilon^{\frac{1}{2}} U_1 + \tilde{d}) R_1],$$

$$(14b) \quad U'_1 = \tilde{b}(\varepsilon U_1 + 1)^2 + \Theta R_1^2 U_1^2 - U_1 [(\varepsilon U_1 + 1)^2 + \Lambda R_1^2 \varepsilon^2 U_1^2],$$

which represents a slow-fast system in standard form for  $\kappa$  small.

When  $\kappa = 0$ , Equation (14) yields the layer problem

$$(15a) \quad R'_1 = 0,$$

$$(15b) \quad U'_1 = \tilde{b}(\varepsilon U_1 + 1)^2 + \Theta R_1^2 U_1^2 - U_1 [(\varepsilon U_1 + 1)^2 + \Lambda R_1^2 \varepsilon^2 U_1^2];$$

considering the limit of  $\varepsilon = 0$  in (15), we obtain

$$(16a) \quad R'_1 = 0,$$

$$(16b) \quad U'_1 = \tilde{b} + \Theta R_1^2 U_1^2 - U_1.$$

The critical manifold for Equation (16) is defined by  $\tilde{b} + \Theta R_1^2 U_1^2 - U_1 = 0$ ; we denote that manifold as  $\mathcal{S}_{00_1}$ . The manifold  $\mathcal{S}_{00_1}$  consists of a left attracting branch  $\mathcal{S}_{00_1}^{a-}$ , where  $U_1 < 2\tilde{b}$ , and a right repelling branch  $\mathcal{S}_{00_1}^r$  with  $U_1 > 2\tilde{b}$ ; these two branches are separated by a fold point at  $A_{00_1} : \left( \frac{1}{2\sqrt{\Theta\tilde{b}}}, 2\tilde{b} \right)$ . The branch  $\mathcal{S}_{00_1}^r$  is asymptotic to the  $U_1$ -axis as  $U_1 \rightarrow \infty$ , while the branch  $\mathcal{S}_{00_1}^{a-}$  intersects the  $U_1$ -axis in the point  $B_{00_1} : (0, \tilde{b})$ . Orbits starting close to the  $U_1$ -axis are rapidly attracted to  $\mathcal{S}_{00_1}^{a-}$ ; they then follow the reduced dynamics until they reach the fold point  $A_{00_1}$ , where they jump in the positive  $U_1$ -direction along an orbit of the layer problem, Equation (15). The geometry in regime  $\mathcal{R}_1$  is summarised in Figure 5; for details on the passage past a singularly perturbed planar fold, the reader is referred to [14], as well as to the summary in Appendix A of [13]. In particular, standard theory [4] implies that  $\mathcal{S}_{00_1}^{a-}$  and  $\mathcal{S}_{00_1}^r$  will persist as slow manifolds away from  $A_{00_1}$ , for  $\kappa$  positive and small.

**Remark 7.** We note that the steady state  $E_{0_\varepsilon}$  is not visible in regime  $\mathcal{R}_1$ : given our choice of  $\mu$  and  $d$ , with  $\frac{\tilde{\mu}}{d} > \frac{1}{2\sqrt{\Theta\tilde{b}}}$ , the equation  $\{\tilde{b} + \Theta R_1^2 U_1^2 - U_1 = 0\}|_{\{R_1 = \frac{\tilde{\mu}}{d}\}}$  admits no real solutions for  $U_1$ ; the underlying reason is the scaling of the  $U$ -coordinate of  $E_{0_\varepsilon}$ , which is identified in regime  $\mathcal{R}_2$  in the subsequent subsection. In particular, it follows that the reduced flow in the  $R_1$ -variable is directed upwards to  $A_{00_1}$  on  $\mathcal{S}_{00_1}$ .

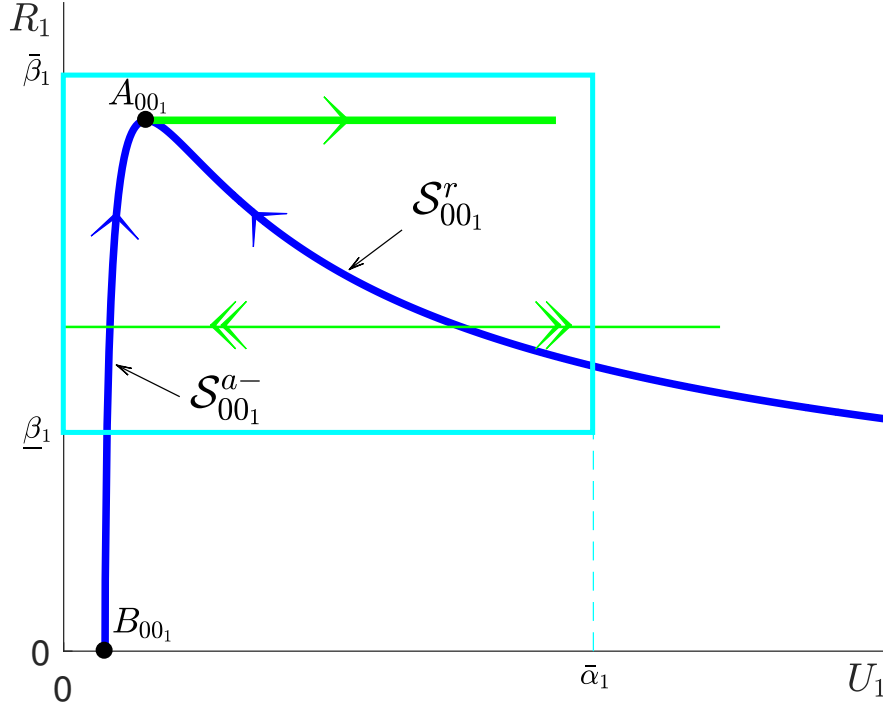


FIGURE 5. Reduced flow on the critical manifold  $\mathcal{S}_{00_1}$  (solid blue) and layer dynamics (solid green) in regime  $\mathcal{R}_1$ .

**Remark 8.** The critical manifold  $\mathcal{S}_{00_1}$  corresponds to appropriately specified portions of  $\mathcal{S}_{0\varepsilon}^{a-}$  and  $\mathcal{S}_{0\varepsilon}^r$ , as defined in Section 2.1, in the limit as  $\varepsilon \rightarrow 0$ , while the fold point  $A_{00_1}$  corresponds to  $A_{0\varepsilon}$  in that limit. (Here, we note that  $\mathcal{S}_{00_1}$  perturbs in a regular fashion for  $\varepsilon$  positive and small.) In some sense, to be specified later, the point  $C_{0\varepsilon}$  is retrieved for  $U_1 \rightarrow \infty$  on  $\mathcal{S}_{0\varepsilon}^r$  in the limit of  $\varepsilon = 0$ .

**3.2. Regime  $\mathcal{R}_2$ :**  $U = \mathcal{O}(\varepsilon)$ ,  $R = \mathcal{O}(\varepsilon^{\frac{1}{2}})$ . Regime  $\mathcal{R}_2$  covers a neighbourhood of the origin  $Q$ ; recall Figure 4. We introduce the scaling

$$(17) \quad R = \varepsilon^{\frac{1}{2}} R_2 \quad \text{and} \quad U = \varepsilon U_2;$$

here, we assume that  $U_2 \in [0, \bar{\alpha}_2]$  and  $R_2 \in [0, \bar{\beta}_2]$ , where  $\bar{\alpha}_2$  and  $\bar{\beta}_2$  are large, corresponding to our assumption that the original variables  $U$  and  $R$  satisfy  $U = \mathcal{O}(\varepsilon)$  and  $R = \mathcal{O}(\varepsilon^{\frac{1}{2}})$ , respectively.

After division through a factor of  $\varepsilon^2$ , Equation (6) becomes

$$(18a) \quad R'_2 = \kappa(U_2 + \mathcal{P}) \frac{(U_2 + 1)^2 + \Lambda \varepsilon R_2^2 U_2^2}{(U_2 + 1)(U_2 + \frac{1}{c})} [\tilde{\mu}(U_2 + 1) - (U_2 + \tilde{d}\varepsilon^{\frac{1}{2}})R_2],$$

$$(18b) \quad U'_2 = \tilde{b}\varepsilon(U_2 + 1)^2 + \Theta R_2^2 U_2^2 - U_2[(U_2 + 1)^2 + \Lambda \varepsilon R_2^2 U_2^2],$$

which again represents a slow-fast system for  $\kappa$  small.

The layer problem obtained for  $\kappa = 0$  now reads

$$(19a) \quad R'_2 = 0,$$

$$(19b) \quad U'_2 = \tilde{b}\varepsilon(U_2 + 1)^2 + \Theta R_2^2 U_2^2 - U_2[(U_2 + 1)^2 + \Lambda \varepsilon R_2^2 U_2^2];$$

setting  $\varepsilon = 0$  in (19), we find the simplified system

$$(20a) \quad R_2' = 0,$$

$$(20b) \quad U_2' = \Theta R_2^2 U_2^2 - U_2(U_2 + 1)^2.$$

The corresponding critical manifold, which is denoted as  $\mathcal{S}_{00_2}$ , is defined by  $\Theta R_2^2 U_2^2 - U_2(U_2 + 1)^2 = 0$ . The manifold  $\mathcal{S}_{00_2}$  consists of a left attracting branch  $\mathcal{S}_{00_2}^{a-}$ , corresponding to  $\{U_2 = 0\}$ , a middle repelling branch  $\mathcal{S}_{00_2}^r$ , with  $0 < U_2 < 1$ , and a right attracting branch  $\mathcal{S}_{00_2}^{a+}$ , where  $U_2 > 1$ . The branches  $\mathcal{S}_{00_2}^r$  and  $\mathcal{S}_{00_2}^{a+}$  are separated by a fold point at  $C_{00_2} : (\frac{2}{\sqrt{\Theta}}, 1)$ . Orbits follow the slow flow on the branch  $\mathcal{S}_{00_2}^{a+}$  until they reach  $C_{00_2}$ , where they jump to a point  $B_{00_2}$  on  $\mathcal{S}_{00_2}^{a-}$  and then follow the slow flow on  $\mathcal{S}_{00_2}^{a-}$ ; see Figure 6 for an illustration. We note that the fold point  $A_{0\varepsilon}$  – and, hence, the fast jump to  $D_{0\varepsilon}$  – is not visible in this regime. Finally, by our assumptions on the parameters  $\Theta$  and  $\mu$ , the steady state at  $E_{00_2} : (\Theta \tilde{\mu}^2, \tilde{\mu} + \frac{1}{\Theta \tilde{\mu}})$  is located on the middle repelling branch  $\mathcal{S}_{00_2}^r$ . (That state is found in the intersection of  $\mathcal{S}_{00_2}$  with the  $R_2$ -nullcline  $\{R_2 = \frac{\tilde{\mu}(U_2+1)}{U_2}\}$ .) Again, geometric singular perturbation theory [4] implies the persistence of  $\mathcal{S}_{00_2}^{a-}$ ,  $\mathcal{S}_{00_2}^r$ , and  $\mathcal{S}_{00_2}^{a+}$  for  $\kappa$  positive and small, uniformly in  $\varepsilon$ , away from the fold point  $C_{00_2}$ , while standard results on passage past a singularly perturbed planar fold [14] apply at  $C_{00_2}$ .

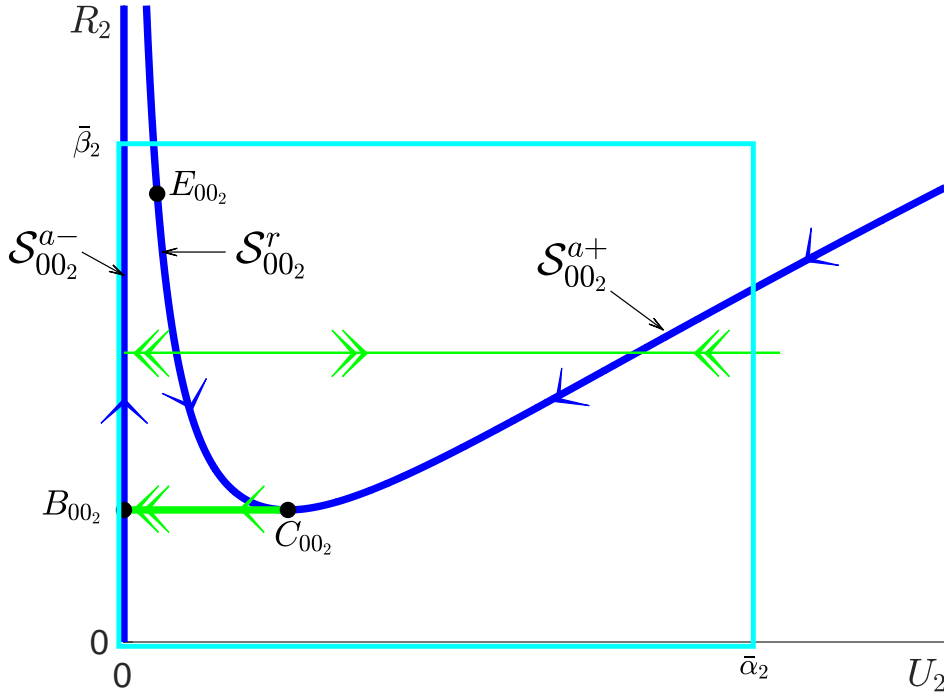


FIGURE 6. Reduced flow on the critical manifold  $\mathcal{S}_{00_2}$  (solid blue), layer dynamics (solid green), and equilibrium  $E_{00_2}$  in regime  $\mathcal{R}_2$ .

**Remark 9.** Figure 2 seems to be in contradiction with Figures 5 and 6, as it indicates that  $E_{0\varepsilon}$  is located near the fold point  $A_{0\varepsilon}$ , rather than close to  $C_{0\varepsilon}$ . However, that seeming discrepancy is due to the fixed, relatively large, value of  $\varepsilon = 0.12$  in Figure 2, recall Table 1, whereas Figures 5 and 6 illustrate the singular limit of  $\varepsilon = 0$ .

**Remark 10.** The critical manifold  $\mathcal{S}_{00_2}$  corresponds to appropriately specified portions of  $\mathcal{S}_{0\varepsilon}^{a-}$ ,  $\mathcal{S}_{0\varepsilon}^r$ , and  $\mathcal{S}_{0\varepsilon}^{a+}$ , as defined in Section 2.1, in the limit as  $\varepsilon \rightarrow 0$ . In particular, the fold point  $C_{00_2}$

corresponds to  $C_{0\varepsilon}$  in that limit, while the point  $B_{00_2}$  is equivalent to  $B_{0\varepsilon}$ . The jump point at  $D_{0\varepsilon}$  corresponds to the limit as  $U_2 \rightarrow \infty$  on  $\mathcal{S}_{00_2}^{a+}$ , while the fold point  $A_{0\varepsilon}$  is found in the limit as  $R_2 \rightarrow \infty$  on  $\mathcal{S}_{00_2}^{a-}$ .

**3.3. Regime  $\mathcal{R}_3$ :**  $U = \mathcal{O}(1)$ ,  $R = \mathcal{O}(1)$ . In regime  $\mathcal{R}_3$ , Equation (6) depends on  $\varepsilon$  in a regular fashion. We consider  $U_3 \in [\underline{\alpha}_3, \bar{\alpha}_3]$  and  $R_3 \in [\underline{\beta}_3, \bar{\beta}_3]$  here, where  $\underline{\alpha}_3$  and  $\underline{\beta}_3$  are positive and small and  $\bar{\alpha}_3$  and  $\bar{\beta}_3$  are assumed to be  $\mathcal{O}(1)$ , corresponding to our assumption that the original variables  $U$  and  $R$  are  $\mathcal{O}(1)$  in the “outer” region. For  $\kappa = 0$  in (6), we obtain the layer problem given in (15), while the limit of  $\varepsilon = 0$  yields the singular layer problem

$$(21a) \quad R'_3 = 0,$$

$$(21b) \quad U'_3 = \Theta R_3^2 U_3^2 - U_3^3 (1 + \Lambda R_3^2).$$

The critical manifold for Equation (21), which we denote as  $\mathcal{S}_{00_3}^{a+}$ , is defined by  $\Theta R_3^2 - U_3(1 + \Lambda R_3^2) = 0$ , and is normally attracting. Since the reduced flow on  $\mathcal{S}_{00_3}^{a+}$  for  $\varepsilon = 0$  reads

$$(22) \quad \dot{R}_3 = -U_3^2 R_3 (1 + \Lambda R_3^2),$$

$R_3$  is decreasing on  $\mathcal{S}_{00_3}^{a+}$ ; see Figure 7.

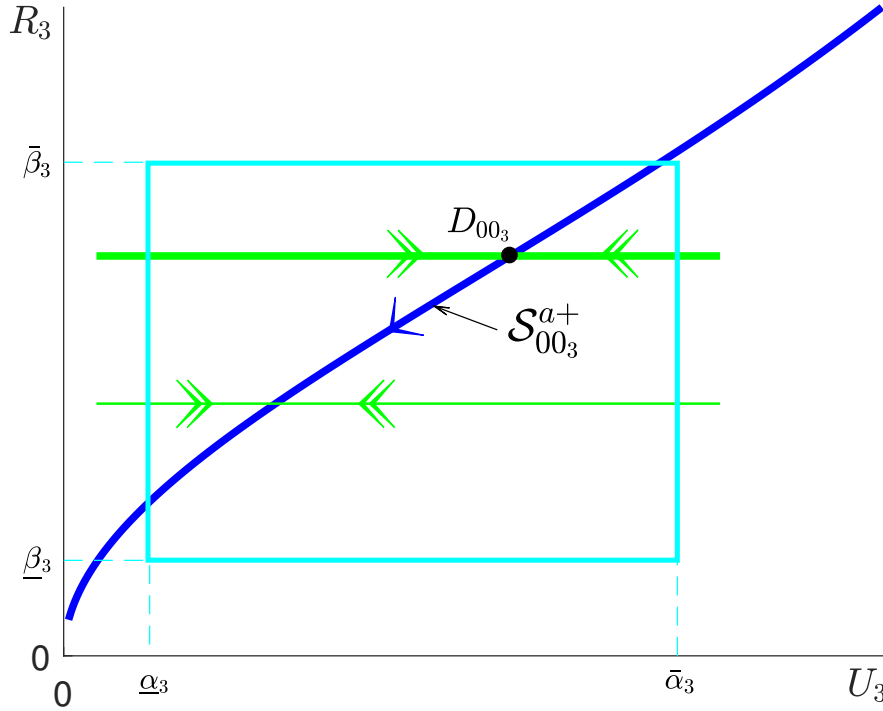


FIGURE 7. Reduced flow on the critical manifold  $\mathcal{S}_{00_3}^{a+}$  (solid blue) and layer dynamics (solid green) in regime  $\mathcal{R}_3$ .

For  $\varepsilon > 0$ , the curve  $\mathcal{S}_{00_3}^{a+}$  perturbs in a regular fashion to the analogue, in regime  $\mathcal{R}_3$ , of the family of saddle-type critical manifolds that was denoted by  $\mathcal{S}_{0\varepsilon}^{a+}$  in Section 2.1. Standard theory [4] implies that orbits to the left of the critical manifold  $\mathcal{S}_{00_3}^{a+}$  are rapidly attracted by the slow manifold corresponding to  $\mathcal{S}_{00_3}^{a+}$ ; they then follow the slow flow on that manifold.

**Remark 11.** In the limit as  $\varepsilon \rightarrow 0$ , the critical manifold  $\mathcal{S}_{00_3}^{a+}$  corresponds to the portion of  $\mathcal{S}_{0\varepsilon}^{a+}$  where  $U_3$  and  $R_3$  are  $\mathcal{O}(1)$ . The point  $D_{00_3}$  corresponds to the point  $D_{0\varepsilon}$  in that limit,

while the singular orbit connecting the point  $A_{00_3}$  – which is not visible in this regime – to  $D_{00_3}$  corresponds to the saddle-type fibre of the point  $D_{0_\varepsilon}$  in the limit as  $\varepsilon \rightarrow 0$ .

**3.4. Summary.** Combining our discussion of the three regimes  $\mathcal{R}_j$  ( $j = 1, 2, 3$ ), we define the singular cycle  $\Gamma_{00}$  for Equation (6) in the limit of  $(\kappa, \varepsilon) = (0, 0)$  as

$$\Gamma_{00} = \Gamma_{00}^{AD} \cup \Gamma_{00}^{DQ} \cup \Gamma_{00}^{QA},$$

where the orbit  $\Gamma_{00}^{AD}$  corresponds to the fast fibre of (8) that connects the points  $A_{00} : \left(\frac{1}{2\sqrt{\Theta\bar{b}}}, 0\right)$  and  $D_{00} : \left(\frac{1}{2\sqrt{\Theta\bar{b}}}, \frac{\Theta}{4\Theta\bar{b}+\Lambda}\right)$ , the orbit  $\Gamma_{00}^{DQ}$  denotes the segment of the critical manifold  $\mathcal{S}_{00}^{a+}$  between the points  $D_{00}$  and  $Q_{00} : (0, 0)$ , and  $\Gamma_{00}^{QA}$  is the segment of the critical manifold  $\mathcal{S}_{00}^r$  between the points  $Q_{00}$  and  $A_{00}$ ; see Figure 8. We emphasise again that no reduced flow can be meaningfully defined on  $\mathcal{S}_{00}^r$ , i.e., that the segment  $\Gamma_{00}^{QA}$  is degenerate; that degeneracy will be partially resolved by blow-up.

For  $(\kappa, \varepsilon) \rightarrow (0, 0)$ , regime  $\mathcal{R}_1$  collapses onto the non-hyperbolic line  $\mathcal{S}_{00}^r$ , while regime  $\mathcal{R}_2$  shrinks to the non-hyperbolic origin; in particular, the points  $B_{00}$  and  $C_{00}$  coalesce into  $Q_{00}$  in the double singular limit, as the fast fibre connecting them vanishes. In regime  $\mathcal{R}_3$ , on the other hand, that limit is regular, as can be seen from the fact that the manifold  $\mathcal{S}_{00}^{a+}$  remains normally attracting.

In conclusion, the degenerate geometry of  $\Gamma_{00}$  has hence been locally resolved in the scaling regimes  $\mathcal{R}_j$  ( $j = 1, 2, 3$ ); however, to obtain a global picture, we investigate the transition between these regimes via a combination of geometric singular perturbation theory and the blow-up technique. Our geometric approach seems ideally suited to such an investigation, as it yields a uniformly valid and intuitively appealing description of relaxation-type oscillation in the two-parameter singular perturbation problem, Equation (6).

**Remark 12.** We note that the lines of equilibria  $\Gamma_{00}^{QA}$  and  $\Gamma_{00}^{DQ}$  for (10) can be connected by the corresponding layer flow for any fixed choice of  $R$ , allowing for a continuum of singular cycles. However, the analysis in regime  $\mathcal{R}_1$  suggests that  $\Gamma_{00}$ , as defined above, is the appropriate choice, which will be substantiated by blow-up in the following section.

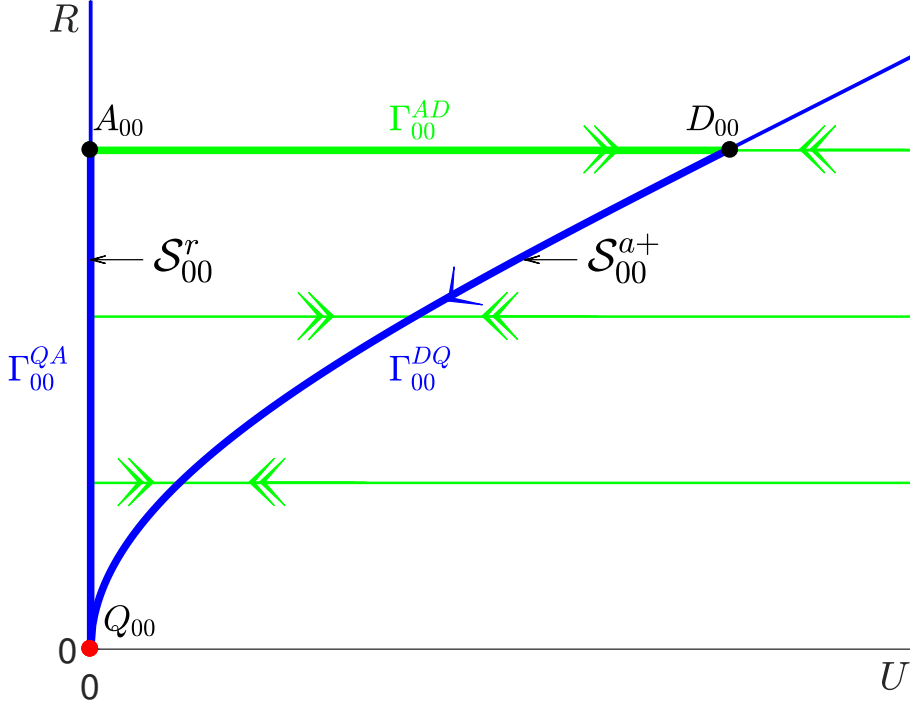


FIGURE 8. Reduced flow on the critical manifold  $\mathcal{S}_{00}$  (solid blue), layer dynamics (solid green), non-hyperbolic origin  $Q_{00}$  (red dot), and singular cycle  $\Gamma_{00}$  (solid blue; solid green) for Equation (10).

#### 4. BLOW-UP ANALYSIS

Given the highly singular nature of Equation (6) in regimes  $\mathcal{R}_1$  and  $\mathcal{R}_2$ , we apply the blow-up technique to desingularise the dynamics in a neighbourhood of the non-hyperbolic  $R$ -axis, with a particular focus on the degenerate equilibrium at the origin. To that end, we consider the augmented vector field that is obtained by appending the trivial equation  $\varepsilon' = 0$  in (6):

$$(23a) \quad R' = \kappa(U + \mathcal{P}\varepsilon) \frac{(U + \varepsilon)^2 + \Lambda R^2 U^2}{(U + \varepsilon)(U + \frac{\varepsilon}{c})} [\tilde{\mu} \varepsilon^{\frac{1}{2}}(U + \varepsilon) - (U + \tilde{d} \varepsilon^{\frac{3}{2}})R],$$

$$(23b) \quad U' = \tilde{b} \varepsilon^2 (U + \varepsilon)^2 + \Theta R^2 U^2 - U[(U + \varepsilon)^2 + \Lambda R^2 U^2],$$

$$(23c) \quad \varepsilon' = 0.$$

As is conventional in the application of blow-up, the parameter  $\varepsilon$  is now treated as an additional state variable in the above augmented system, while  $\kappa$  encodes the separation of scales, as before. Our analysis will proceed in two steps: first, we will blow up the origin in the extended  $(R, U, \varepsilon)$ -space to a sphere, which will allow us to give a rigorous description of the dynamics in regime  $\mathcal{R}_2$ ; the non-hyperbolic line  $\mathcal{S}_{00}^r$  – which corresponds to regime  $\mathcal{R}_1$  – will be recovered in one of the phase-directional charts in that blow up, and will be desingularised via a second (cylindrical) blow-up transformation. The dynamics that is obtained in the various coordinate charts after blow-up will then be combined into a global description of the flow of Equation (6) near the degenerate  $R$ -axis that is uniformly valid in both  $\kappa$  and  $\varepsilon$ .

Finally, we note that the phase space of (6) can be viewed as being foliated in  $\varepsilon \in [0, \varepsilon_0]$ , for  $\varepsilon_0$  positive and small. Correspondingly, the family of critical manifolds  $\mathcal{S}_{0\varepsilon} = \mathcal{S}_{0\varepsilon}^{a-} \cup \mathcal{S}_{0\varepsilon}^r \cup \mathcal{S}_{0\varepsilon}^{a+}$  defined in Section 2.1 can be viewed as a two-dimensional critical manifold  $\mathcal{S}_0$ , with folds along the curves  $\mathcal{F}_0^A := \{(A_{0\varepsilon}, \varepsilon) \mid \varepsilon \in [0, \varepsilon_0]\}$  and  $\mathcal{F}_0^C := \{(C_{0\varepsilon}, \varepsilon) \mid \varepsilon \in [0, \varepsilon_0]\}$ .



**4.1. Blow-up of the degenerate origin.** We recall that regime  $\mathcal{R}_2$  corresponds to the scaling  $U = \mathcal{O}(\varepsilon)$  and  $R = \mathcal{O}(\varepsilon^{\frac{1}{2}})$ ; cf. Section 3.2. In view of these scalings, we introduce the following quasi-homogeneous blow-up transformation of the origin in Equation (23):

$$(24) \quad R = \rho \bar{r}, \quad U = \rho^2 \bar{u}, \quad \text{and} \quad \varepsilon = \rho^2 \bar{\varepsilon},$$

with  $(\bar{r}, \bar{u}, \bar{\varepsilon}) \in \mathbb{S}^2$  and  $\rho \in [0, \rho_0]$ , for  $\rho_0$  positive and small. In other words, the degenerate origin in  $(R, U, \varepsilon)$ -space corresponding to  $\rho = 0$  in Equation (24) is blown up to the 2-sphere in  $\mathbb{R}^3$ . The vector field that is induced by Equation (23) after blow-up is conventionally studied in appropriate coordinate charts [3, 14] that cover different parts of the blown-up space. We will require two charts in our analysis, which we denote by  $K_1$  and  $K_2$ ; these charts are obtained for  $\bar{r} = 1$  and  $\bar{\varepsilon} = 1$  in (24), respectively, which implies

$$(25) \quad R = \rho_1, \quad U = \rho_1^2 u_1, \quad \text{and} \quad \varepsilon = \rho_1^2 \varepsilon_1$$

and

$$(26) \quad R = \rho_2 r_2, \quad U = \rho_2^2 u_2, \quad \text{and} \quad \varepsilon = \rho_2^2,$$

respectively, for the coordinates in these charts. Intuitively speaking, chart  $K_1$  hence covers a neighbourhood of parts of the equator of the blow-up sphere  $\mathbb{S}^2 \times \{0\}$  where  $R > 0$  holds, while the top of that sphere, with  $\varepsilon > 0$ , is described in chart  $K_2$ ; see Figure 12 below for an illustration.

**Remark 13.** For any object  $\square_{\kappa\varepsilon}$  given in the original  $(R, U, \varepsilon)$ -variables, we denote the corresponding blown-up object by  $\bar{\square}_{\kappa}$ . Moreover, in chart  $K_i$ , that object will be denoted by  $\square_{\kappa_i}$ .

**Lemma 1.** *The change-of-coordinates transformation  $\mathcal{K}_{12}$  between charts  $K_1$  and  $K_2$  is given by*

$$\mathcal{K}_{12} : (\rho_1, u_1, \varepsilon_1) \mapsto \left( \rho_2 r_2, \frac{u_2}{r_2^2}, \frac{1}{r_2^2} \right);$$

its inverse  $\mathcal{K}_{21} = \mathcal{K}_{12}^{-1}$  reads

$$\mathcal{K}_{21} : (r_2, u_2, \rho_2) \mapsto \left( \frac{1}{\sqrt{\varepsilon_1}}, \frac{u_1}{\varepsilon_1}, \rho_1 \sqrt{\varepsilon_1} \right).$$

We will first consider the dynamics in the “rescaling” chart  $K_2$ ; then, we will study the flow in the “phase-directional” chart  $K_1$ . In particular, the latter will allow us to describe the transition between the “inner” and “outer” regions, which correspond to regimes  $\mathcal{R}_2$  and  $\mathcal{R}_3$ , respectively, as defined in Section 3.

**4.2. Dynamics in chart  $K_2$ .** In chart  $K_2$ , the blow-up transformation defined in (24) is given by (26); substituting into Equation (23), we find

$$(27a) \quad r_2' = \kappa \rho_2^4 (u_2 + \mathcal{P}) \frac{(u_2 + 1)^2 + \Lambda \rho_2^2 r_2^2 u_2^2}{(u_2 + 1)(u_2 + \frac{1}{c})} [\tilde{\mu}(u_2 + 1) - (u_2 + \tilde{d}\rho_2)r_2],$$

$$(27b) \quad u_2' = \rho_2^4 \left\{ \tilde{b}\rho_2^2 (u_2 + 1)^2 + \Theta r_2^2 u_2^2 - u_2 [(u_2 + 1)^2 + \Lambda \rho_2^2 r_2^2 u_2^2] \right\},$$

$$(27c) \quad \rho_2' = 0.$$

By dividing out a factor of  $\rho_2^4$  from the right-hand sides in Equation (27), we obtain the desingularised dynamics in chart  $K_2$ :

$$(28a) \quad r_2' = \kappa (u_2 + \mathcal{P}) \frac{(u_2 + 1)^2 + \Lambda \rho_2^2 r_2^2 u_2^2}{(u_2 + 1)(u_2 + \frac{1}{c})} [\tilde{\mu}(u_2 + 1) - (u_2 + \tilde{d}\rho_2)r_2],$$

$$(28b) \quad u_2' = \tilde{b}\rho_2^2 (u_2 + 1)^2 + \Theta r_2^2 u_2^2 - u_2 [(u_2 + 1)^2 + \Lambda \rho_2^2 r_2^2 u_2^2],$$

$$(28c) \quad \rho_2' = 0,$$

which is a slow-fast system in standard form, with singular perturbation parameter  $\kappa$ ; correspondingly, the variable  $r_2$  is slow, while  $u_2$  is fast. We observe that  $K_2$  corresponds precisely

to regime  $\mathcal{R}_2$ , as Equation (28) is equivalent to (18), with  $(R_2, U_2) = (r_2, u_2)$ ,  $\varepsilon = \rho_2^2$ , and the (trivial) equation  $\rho_2' = 0$  appended. Hence, the geometric singular perturbation analysis in chart  $K_2$  proceeds as in Section 3.2; the relevant dynamics in blown-up space is again illustrated in Figure 6. In particular, it follows that the geometry of Equation (28) described in Section 3.2 is valid on compact domains in  $K_2$ .

We first consider the flow of Equation (28) in the invariant plane  $\{\rho_2 = 0\}$ , which is governed by

$$(29a) \quad r_2' = \kappa(u_2 + \mathcal{P}) \frac{u_2 + 1}{u_2 + \frac{1}{c}} [\tilde{\mu}(u_2 + 1) - u_2 r_2],$$

$$(29b) \quad u_2' = \Theta r_2^2 u_2^2 - u_2(u_2 + 1)^2,$$

$$(29c) \quad \rho_2' = 0.$$

Equation (29) is again a slow-fast system in standard form, with singular perturbation parameter  $\kappa$ ; correspondingly, the variable  $r_2$  is slow, while  $u_2$  is fast. The corresponding layer problem reads

$$(30a) \quad r_2' = 0,$$

$$(30b) \quad u_2' = \Theta r_2^2 u_2^2 - u_2(u_2 + 1)^2,$$

$$(30c) \quad \rho_2' = 0.$$

It follows immediately from Section 3.2 that the critical manifold for Equation (30) consists of the three branches  $\mathcal{S}_{0_2}^{a-}$ ,  $\mathcal{S}_{0_2}^r$ , and  $\mathcal{S}_{0_2}^{a+}$ ; the former equals a segment of the  $r_2$ -axis, and is normally attracting under the flow of (30). The branches  $\mathcal{S}_{0_2}^r$  and  $\mathcal{S}_{0_2}^{a+}$  are separated by the fold point  $C_{0_2}$  at which hyperbolicity is lost;  $\mathcal{S}_{0_2}^r$  is normally repelling, while  $\mathcal{S}_{0_2}^{a+}$  is normally attracting, outside of a neighbourhood of that point. See again Figure 6 for an illustration; here, the notation  $\square_{0_2}$  in chart  $K_2$  corresponds to  $\square_{00_2}$  in regime  $\mathcal{R}_2$ .

**4.3. Dynamics in chart  $K_1$ .** In chart  $K_1$ , the blow-up transformation defined in Equation (24) is given by (25). Substituting into Equation (23), dividing out a factor of  $\rho_1^4$  from the resulting equations, as before, and setting

$$F_1(\rho_1, u_1, \varepsilon_1) = (u_1 + \mathcal{P}\varepsilon_1) \frac{(u_1 + \varepsilon_1)^2 + \Lambda \rho_1^2 u_1^2}{(u_1 + \varepsilon_1)(u_1 + \frac{\varepsilon_1}{c})} \left[ \tilde{\mu} \varepsilon_1^{\frac{1}{2}} (u_1 + \varepsilon_1) - \left( u_1 + \tilde{d} \rho_1 \varepsilon_1^{\frac{3}{2}} \right) \right],$$

we obtain the system

$$(31a) \quad \rho_1' = \kappa \rho_1 F_1(\rho_1, u_1, \varepsilon_1),$$

$$(31b) \quad u_1' = \tilde{b} \rho_1^2 \varepsilon_1^2 (u_1 + \varepsilon_1)^2 + \Theta u_1^2 - u_1 [(u_1 + \varepsilon_1)^2 + \Lambda \rho_1^2 u_1^2] - 2\kappa u_1 F_1(\rho_1, u_1, \varepsilon_1),$$

$$(31c) \quad \varepsilon_1' = -2\kappa \varepsilon_1 F_1(\rho_1, u_1, \varepsilon_1),$$

which is a slow-fast system with singular perturbation parameter  $\kappa$ ; correspondingly, the variables  $\rho_1$  and  $\varepsilon_1$  are slow, while  $u_1$  is fast.

**Remark 14.** *A priori*, it may seem that the denominator  $(u_1 + \varepsilon_1)(u_1 + \frac{\varepsilon_1}{c})$  in  $F_1(\rho_1, u_1, \varepsilon_1)$  may cause non-uniformity in the limit as  $(u_1, \varepsilon_1) \rightarrow (0, 0)$ . However, one can show that  $F_1$  vanishes to the order  $\mathcal{O}(2)$  at  $(u_1, \varepsilon_1) = (0, 0)$ , which is sufficient for our purposes.

Setting  $\kappa = 0$  in Equation (31) gives the layer problem

$$(32a) \quad \rho_1' = 0,$$

$$(32b) \quad u_1' = \tilde{b} \rho_1^2 \varepsilon_1^2 (u_1 + \varepsilon_1)^2 + \Theta u_1^2 - u_1 [(u_1 + \varepsilon_1)^2 + \Lambda \rho_1^2 u_1^2],$$

$$(32c) \quad \varepsilon_1' = 0;$$

the corresponding critical manifold  $\mathcal{S}_{0_1}$  is the hypersurface in  $(\rho_1, u_1, \varepsilon_1)$ -space that is defined by

$$(33) \quad \tilde{b} \rho_1^2 \varepsilon_1^2 (u_1 + \varepsilon_1)^2 + \Theta u_1^2 - u_1 [(u_1 + \varepsilon_1)^2 + \Lambda \rho_1^2 u_1^2] = 0.$$

Rather than attempting a global description of  $\mathcal{S}_{0_1}$ , we will restrict ourselves to the two invariant hyperplanes  $\{\rho_1 = 0\}$  and  $\{\varepsilon_1 = 0\}$  for Equation (31), which will allow us to infer the geometry of  $\mathcal{S}_{0_1}$  for either  $\rho_1$  or  $\varepsilon_1$  small. The flow in the plane  $\{\rho_1 = 0\}$  is governed by

$$(34a) \quad u_1' = \Theta u_1^2 - u_1(u_1 + \varepsilon_1)^2 - 2\kappa u_1 F_1(0, u_1, \varepsilon_1),$$

$$(34b) \quad \varepsilon_1' = -2\kappa \varepsilon_1 F_1(0, u_1, \varepsilon_1),$$

with

$$F_1(0, u_1, \varepsilon_1) = (u_1 + \mathcal{P}\varepsilon_1) \frac{u_1 + \varepsilon_1}{u_1 + \frac{\varepsilon_1}{c}} \left[ \tilde{\mu} \varepsilon_1^{\frac{1}{2}} (u_1 + \varepsilon_1) - u_1 \right].$$

(One can again show that  $F_1(0, u_1, \varepsilon_1)$  vanishes to the order  $\mathcal{O}(2)$  at  $(u_1, \varepsilon_1) = (0, 0)$ ; recall Remark 14.) Setting  $\kappa = 0$  in Equation (34), we obtain the layer problem

$$(35a) \quad u_1' = \Theta u_1^2 - u_1(u_1 + \varepsilon_1)^2,$$

$$(35b) \quad \varepsilon_1' = 0.$$

The critical manifold of Equation (35), which is denoted by  $\hat{\mathcal{S}}_{0_1}$ , is defined by  $u_1[\Theta u_1 - (u_1 + \varepsilon_1)^2] = 0$ ; it consists of a normally attracting left branch  $\hat{\mathcal{S}}_{0_1}^-$  corresponding to the invariant line  $\{u_1 = 0\}$  with  $\varepsilon_1$  positive, a normally repelling middle branch  $\hat{\mathcal{S}}_{0_1}^r$  that corresponds to  $u_1 \in (0, \frac{\Theta}{4})$ , and a normally attracting right branch  $\hat{\mathcal{S}}_{0_1}^{a+}$  corresponding to  $u_1 \in (\frac{\Theta}{4}, \Theta]$ . The branches  $\hat{\mathcal{S}}_{0_1}^r$  and  $\hat{\mathcal{S}}_{0_1}^{a+}$  are separated by the fold point  $C_{0_1}$ ; the equilibrium  $E_{0_1}$ , which is easily obtained from (33), lies on  $\hat{\mathcal{S}}_{0_1}^r$  due to our assumptions on the parameters  $\Theta$  and  $\mu$ , while  $\hat{\mathcal{S}}_{0_1}^-$  and  $\hat{\mathcal{S}}_{0_1}^r$  intersect in the origin  $\hat{P}_1 : (0, 0, 0)$ . (We note that, clearly, all three branches of  $\hat{\mathcal{S}}_{0_1}$  are intersections of  $\mathcal{S}_{0_1}$  with the plane  $\{\rho_1 = 0\}$ .) From the corresponding reduced problem, we see that  $\varepsilon_1$  increases above  $E_{0_1}$  on  $\hat{\mathcal{S}}_{0_1}^r$  and on  $\hat{\mathcal{S}}_{0_1}^{a+}$ , while it decreases below  $E_{0_1}$  on  $\hat{\mathcal{S}}_{0_1}^r$  and on  $\hat{\mathcal{S}}_{0_1}^-$ . Hence, orbits follow the slow manifold  $\hat{\mathcal{S}}_{0_1}^{a+}$  until they reach the fold point at  $C_{0_1}$ , where they jump to the point  $B_{0_1} : (0, 0, \frac{\Theta}{4}) \in \hat{\mathcal{S}}_{0_1}^-$ . The geometry in  $\{\rho_1 = 0\}$  is summarised in Figure 9.

In the invariant plane  $\{\varepsilon_1 = 0\}$ ,  $F_1(\rho_1, u_1, 0) = -u_1^2(1 + \Lambda\rho_1^2)$  implies

$$(36a) \quad \rho_1' = -\kappa\rho_1 u_1^2(1 + \Lambda\rho_1^2),$$

$$(36b) \quad u_1' = u_1^2[\Theta - u_1(1 + \Lambda\rho_1^2)] + 2\kappa u_1^3(1 + \Lambda\rho_1^2),$$

which, for  $\kappa = 0$ , yields the layer problem

$$(37a) \quad \rho_1' = 0,$$

$$(37b) \quad u_1' = u_1^2[\Theta - u_1(1 + \Lambda\rho_1^2)].$$

The critical manifold for Equation (37), which is denoted by  $\check{\mathcal{S}}_{0_1}$ , is defined by  $u_1^2[\Theta - u_1(1 + \Lambda\rho_1^2)] = 0$ . A straightforward calculation shows that  $\check{\mathcal{S}}_{0_1}$  consists of a right attracting branch  $\check{\mathcal{S}}_{0_1}^{a+}$  corresponding to the invariant curve  $u_1 = \frac{\Theta}{1 + \Lambda\rho_1^2}$  and the non-hyperbolic line  $\check{\ell}_{0_1}$ , given by  $\{u_1 = 0\}$ . Both branches of  $\check{\mathcal{S}}_{0_1}$  are intersections of the critical manifold  $\mathcal{S}_{0_1}$  for Equation (32) with the plane  $\{\varepsilon_1 = 0\}$ . From the corresponding reduced problem, we find that  $\rho_1$  is decreasing on  $\check{\mathcal{S}}_{0_1}^{a+}$ . Finally, the curves  $\check{\mathcal{S}}_{0_1}^{a+}$  and  $\check{\mathcal{S}}_{0_1}^{a+}$  intersect on the  $u_1$ -axis at the point  $\check{Q}_1 : (0, \Theta, 0)$ ; see again Figure 9 for an illustration.

**Remark 15.** We emphasise that the critical manifold  $\hat{\mathcal{S}}_{0_1}$  and the fold point  $C_{0_1}$  for Equation (35) were already identified in chart  $K_2$ , and that they are hence merely recovered in  $K_1$ .

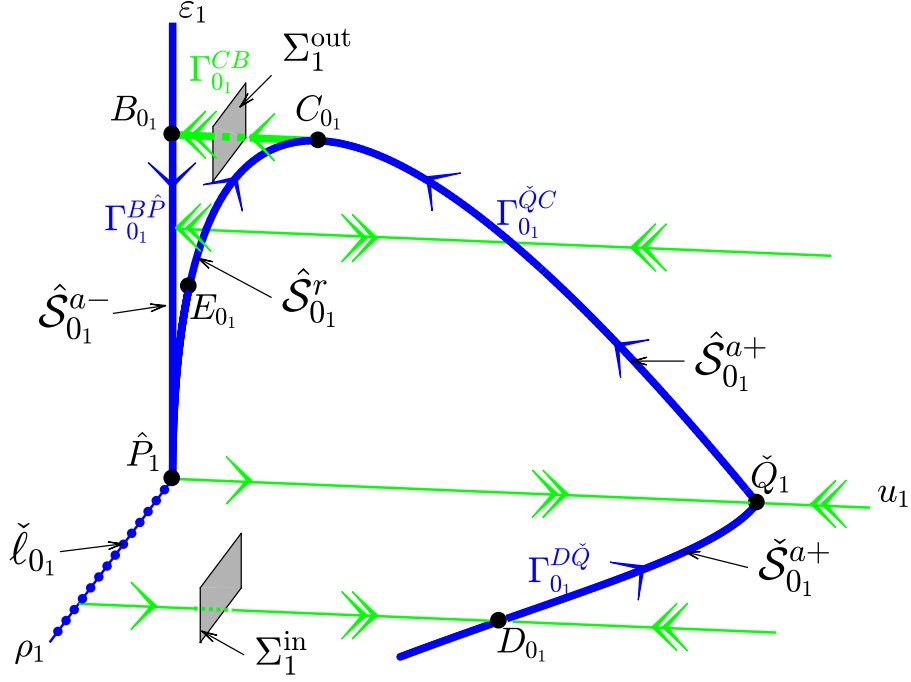


FIGURE 9. Geometry in  $\{\rho_1 = 0\}$  and  $\{\varepsilon_1 = 0\}$ , for  $\kappa = 0$ , in chart  $K_1$ : reduced flow (solid blue), layer dynamics (solid green), and equilibrium  $E_{0_1}$ .

We may summarise the above discussion as follows:

**Lemma 2.** *For  $\rho_1$  or  $\varepsilon_1$  sufficiently small, the critical manifold  $\mathcal{S}_{0_1}$  that is defined by Equation (33) has the following properties:*

- i. *The manifold  $\mathcal{S}_{0_1} = \mathcal{S}_{0_1}^{a-} \cup \mathcal{S}_{0_1}^r \cup \mathcal{F}_{0_1}^C \cup \mathcal{S}_{0_1}^{a+}$  is smooth away from the line  $\check{\ell}_{0_1}$ .*
- ii. *The manifold  $\mathcal{S}_{0_1}$  has a folded structure; specifically, it is divided by the fold curve  $\mathcal{F}_{0_1}^C$  into two branches  $\mathcal{S}_{0_1}^r$  and  $\mathcal{S}_{0_1}^{a+}$ , whereas the branches  $\mathcal{S}_{0_1}^{a-}$  and  $\mathcal{S}_{0_1}^r$  intersect cusp-like along  $\check{\ell}_{0_1}$ .*
- iii. *The branches  $\mathcal{S}_{0_1}^{a-}$  and  $\mathcal{S}_{0_1}^{a+}$  are attracting under the layer flow of Equation (32), while the branch  $\mathcal{S}_{0_1}^r$  is repelling.*
- iv. *The restriction of  $\mathcal{S}_{0_1}^{a-}$ ,  $\mathcal{S}_{0_1}^r$ , and  $\mathcal{S}_{0_1}^{a+}$  to the invariant hyperplane  $\{\rho_1 = 0\}$  corresponds to  $\hat{\mathcal{S}}_{0_1}^{a-}$ ,  $\hat{\mathcal{S}}_{0_1}^r$ , and  $\hat{\mathcal{S}}_{0_1}^{a+}$ , respectively; correspondingly, the fold curve  $\mathcal{F}_{0_1}^C$  reduces to the point  $C_{0_1}$ .*
- v. *In the invariant hyperplane  $\{\varepsilon_1 = 0\}$ ,  $\mathcal{S}_{0_1}^{a-}$  and  $\mathcal{S}_{0_1}^r$  coalesce into  $\check{\ell}_{0_1}$ , while  $\mathcal{S}_{0_1}^{a+}$  corresponds to  $\check{\mathcal{S}}_{0_1}^{a+}$  in that limit.*

*Proof.* Outside of a neighbourhood of the line  $\check{\ell}_{0_1}$ , the above assertions follow from the Implicit Function Theorem, in combination with the structural stability of folds; see [13] and the references therein for details. The geometry of the manifold  $\mathcal{S}_{0_1}$  near  $\check{\ell}_{0_1}$ , and the corresponding dynamics of Equation (31), will be considered in Section 4.4 below.  $\square$

For future reference, we define the sections  $\Sigma_1^{\text{in}}$  and  $\Sigma_1^{\text{out}}$  for the flow of Equation (31) as

$$(38a) \quad \Sigma_1^{\text{in}} := \left\{ (\rho_1, \frac{\Theta}{4}, \varepsilon_1) \mid \rho_1 - \frac{1}{2\sqrt{\Theta\check{b}}} \in [\rho_*, \rho^*], \varepsilon_1 \in [\varepsilon_*, \varepsilon^*] \right\} \quad \text{and}$$

$$(38b) \quad \Sigma_1^{\text{out}} := \left\{ (\rho_1, \frac{\Theta}{8}, \varepsilon_1) \mid \rho_1 \in [\rho_*, \rho^*], \varepsilon_1 - \frac{\Theta}{4} \in [\varepsilon_*, \varepsilon^*] \right\},$$

respectively; see Figure 9. (Here,  $\rho_*$ ,  $\rho^*$ ,  $\varepsilon_*$ , and  $\varepsilon^*$  are suitably chosen constants.)

The situation in chart  $K_1$  can be summarised as follows: the segment  $\Gamma_{0_1}^{D\check{Q}}$  of the singular orbit is initialised close to a point  $D_{0_1}$  which will be specified in chart  $K_4$  in the following section; the orbit is attracted to  $\check{S}_{0_1}^{a+}$  and then follows the slow flow thereon until it reaches the point  $\check{Q}_1$ . The continuation of  $\Gamma_{0_1}^{D\check{Q}}$  past  $\check{Q}_1$  is given by the orbit  $\Gamma_{0_1}^{\check{Q}C}$  along the slow flow on  $\hat{S}_{0_1}^{a+}$  to the fold point  $C_{0_1}$ , where the orbit  $\Gamma_{0_1}^{CB}$  represents the jump along the fast flow to the point  $B_{0_1}$  on  $\hat{S}_{0_1}^{a-}$ ; the orbit  $\Gamma_{0_1}^{B\hat{P}}$  then follows the slow flow on  $\hat{S}_{0_1}^{a-}$  to the origin  $\hat{P}_1$ , which is still a non-hyperbolic steady state for (31). The continuation of the orbit is located on the degenerate (non-hyperbolic) line  $\check{\ell}_{0_1}$ ; to resolve that degeneracy, we require a further blow-up transformation, which is introduced in the subsequent subsection. The geometry in the hyperplanes  $\{\rho_1 = 0\}$  and  $\{\varepsilon_1 = 0\}$  in chart  $K_1$  is illustrated in Figure 9.

**4.4. Blow-up of the non-hyperbolic line  $\check{\ell}_{0_1}$ .** To analyse the dynamics in a neighbourhood of the non-hyperbolic line  $\check{\ell}_{0_1}$  recovered in chart  $K_1$ , we introduce the quasi-homogeneous, cylindrical blow-up transformation

$$(39) \quad \rho_1 = \bar{r}, \quad u_1 = \delta^2 \bar{u}, \quad \text{and} \quad \varepsilon_1 = \delta \bar{\varepsilon},$$

with  $\bar{r} \in \mathbb{R}^+$ ,  $(\bar{u}, \bar{\varepsilon}) \in \mathbb{S}^1$ , and  $\delta \in [0, \delta_0]$ , for  $\delta_0$  positive and small; in other words, the line  $\check{\ell}_{0_1}$  is blown up to the cylinder  $\mathbb{R}^+ \times \mathbb{S}^1 \times \{0\}$ . We emphasise that this second blow-up is performed entirely in chart  $K_1$ .

The vector field that is induced by Equation (31) is studied in two coordinate charts  $K_3$  and  $K_4$ , which are obtained for  $\bar{\varepsilon} = 1$  and  $\bar{u} = 1$  in (39), respectively; see again [3, 14] for details. Hence, we have

$$(40) \quad \rho_1 = r_3, \quad u_1 = \delta_3^2 u_3, \quad \text{and} \quad \varepsilon_1 = \delta_3$$

and

$$(41) \quad \rho_1 = r_4, \quad u_1 = \delta_4^2, \quad \text{and} \quad \varepsilon_1 = \delta_4 \varepsilon_4,$$

respectively, for the coordinates in these charts. Intuitively, chart  $K_3$  covers the top of the cylinder  $\mathbb{R}^+ \times \mathbb{S}^1 \times \{0\}$  corresponding to  $\bar{\varepsilon}$  positive, while the flow in a neighbourhood of the front of that cylinder, with  $\bar{u}$  positive, is described in chart  $K_4$ ; cf. again Figure 12 below.

**Lemma 3.** *The change-of-coordinates transformation  $\mathcal{K}_{34}$  between charts  $K_3$  and  $K_4$  is given by*

$$\mathcal{K}_{34} : (r_3, u_3, \delta_3) \mapsto \left( r_4, \frac{1}{\varepsilon_4^2}, \delta_4 \varepsilon_4 \right);$$

its inverse  $\mathcal{K}_{43} = \mathcal{K}_{34}^{-1}$  reads

$$\mathcal{K}_{43} : (r_4, \delta_4, \varepsilon_4) \mapsto \left( r_3, \sqrt{u_3} \delta_3, \frac{1}{\sqrt{u_3}} \right).$$

As will become clear in the following, chart  $K_3$  covers the transition between regimes  $\mathcal{R}_1$  and  $\mathcal{R}_2$ , while the transition between  $\mathcal{R}_1$  and  $\mathcal{R}_3$  is naturally described in chart  $K_4$ ; both charts provide sufficient overlap for matching to be accomplished between the respective scaling regimes.

**4.5. Dynamics in chart  $K_3$ .** In chart  $K_3$ , the blow-up transformation defined by  $\bar{\varepsilon} = 1$  in Equation (39) is given as in (40). Substituting into Equation (31), dividing out the factor  $\delta_3^2$  from the resulting equations, and defining

$$\begin{aligned} F_3(r_3, u_3, \delta_3) = F_1(r_3, \delta_3^2 u_3, \delta_3) \delta_3^{-2} &= \delta_3^{\frac{1}{2}} (\delta_3 u_3 + \mathcal{P}) \frac{(\delta_3 u_3 + 1)^2 + \Lambda r_3^2 \delta_3^2 u_3^2}{(\delta_3 u_3 + 1)(\delta_3 u_3 + \frac{1}{c})} \\ &\quad \times \left[ \tilde{\mu}(\delta_3 u_3 + 1) - \left( \delta_3^{\frac{1}{2}} u_3 + \tilde{d} r_3 \right) \right], \end{aligned}$$

we obtain the system

$$(42a) \quad r'_3 = \kappa r_3 F_3(r_3, u_3, \delta_3),$$

$$(42b) \quad u'_3 = \tilde{b}r_3^2(\delta_3 u_3 + 1)^2 + \Theta u_3^2 - u_3[(\delta_3 u_3 + 1)^2 + \Lambda r_3^2 \delta_3^2 u_3^2] + 2\kappa u_3 F_3(r_3, u_3, \delta_3),$$

$$(42c) \quad \delta'_3 = -2\kappa \delta_3 F_3(r_3, u_3, \delta_3),$$

which is a slow-fast system with singular perturbation parameter  $\kappa$ ; correspondingly, the variables  $r_3$  and  $\delta_3$  are slow, while  $u_3$  is fast. Here, the prime now denotes differentiation with respect to a new independent variable. For  $\kappa = 0$  in (42), one obtains the layer problem

$$(43a) \quad r'_3 = 0,$$

$$(43b) \quad u'_3 = \tilde{b}r_3^2(\delta_3 u_3 + 1)^2 + \Theta u_3^2 - u_3[(\delta_3 u_3 + 1)^2 + \Lambda r_3^2 \delta_3^2 u_3^2],$$

$$(43c) \quad \delta'_3 = 0.$$

The corresponding critical manifold  $\mathcal{S}_{0_3}$  is the hypersurface in  $(r_3, u_3, \delta_3)$ -space that is defined by

$$(44) \quad \tilde{b}r_3^2(\delta_3 u_3 + 1)^2 + \Theta u_3^2 - u_3[(\delta_3 u_3 + 1)^2 + \Lambda r_3^2 \delta_3^2 u_3^2] = 0.$$

The flow of Equation (42) in the invariant plane  $\{r_3 = 0\}$  is governed by

$$(45a) \quad u'_3 = \Theta u_3^2 - u_3(\delta_3 u_3 + 1)^2 + 2\kappa u_3 F_3(0, u_3, \delta_3),$$

$$(45b) \quad \delta'_3 = -2\kappa \delta_3 F_3(0, u_3, \delta_3),$$

with

$$F_3(0, u_3, \delta_3) = \delta_3^{\frac{1}{2}}(\delta_3 u_3 + \mathcal{P}) \frac{\delta_3 u_3 + 1}{\delta_3 u_3 + \frac{1}{c}} \left[ \tilde{\mu}(\delta_3 u_3 + 1) - \delta_3^{\frac{1}{2}} u_3 \right],$$

which is again a slow-fast system with respect to  $\kappa$ ; correspondingly, the variable  $\delta_3$  is slow, while  $u_3$  is a fast variable. Setting  $\kappa = 0$ , we obtain the layer problem

$$(46a) \quad u'_3 = \Theta u_3^2 - u_3(\delta_3 u_3 + 1)^2,$$

$$(46b) \quad \delta'_3 = 0.$$

The critical manifold in the plane  $\{r_3 = 0\}$ , which we denote by  $\hat{\mathcal{S}}_{0_3}$ , is defined by  $u_3[\Theta u_3 - (\delta_3 u_3 + 1)^2] = 0$ . It consists of an attracting left branch  $\hat{\mathcal{S}}_{0_3}^{a-}$  – the  $\delta_3$ -axis, a repelling middle branch  $\hat{\mathcal{S}}_{0_3}^r$ , and an attracting right branch  $\hat{\mathcal{S}}_{0_3}^{a+}$ . The branches  $\hat{\mathcal{S}}_{0_3}^r$  and  $\hat{\mathcal{S}}_{0_3}^{a+}$  are separated by a fold point at  $C_{0_3}$ ; here, we note that the equilibrium  $E_{0_3}$  lies in  $\hat{\mathcal{S}}_{0_3}^r$ . Moreover,  $\hat{\mathcal{S}}_{0_3}^{a-}$  and  $\hat{\mathcal{S}}_{0_3}^r$  intersect the  $u_3$ -axis in the points  $\hat{P}_3 : (0, 0, 0)$  and  $\hat{Q}_3 : (0, \frac{1}{\Theta}, 0)$ , respectively. All three branches of  $\hat{\mathcal{S}}_{0_3}$  are intersections of  $\mathcal{S}_{0_3}$  with the plane  $\{r_3 = 0\}$ . From the corresponding reduced problem, we conclude that  $\delta_3$  is increasing on  $\hat{\mathcal{S}}_{0_3}^r$  above  $E_{0_3}$  and on  $\hat{\mathcal{S}}_{0_3}^{a+}$ , while it is decreasing on  $\hat{\mathcal{S}}_{0_3}^r$  below  $E_{0_3}$  and on  $\hat{\mathcal{S}}_{0_3}^{a-}$ . Hence, orbits follow the slow manifold  $\hat{\mathcal{S}}_{0_3}^{a+}$  until they reach the fold point  $C_{0_3}$ , where they jump to the point  $B_{0_3} \in \hat{\mathcal{S}}_{0_3}^{a-}$ .

Next, we consider the flow of Equation (42) in the invariant plane  $\{\delta_3 = 0\}$ , which is governed by

$$(47a) \quad r'_3 = 0,$$

$$(47b) \quad u'_3 = \tilde{b}r_3^2 + \Theta u_3^2 - u_3.$$

The corresponding critical manifold, which is denoted by  $\check{\mathcal{S}}_{0_3}$ , is defined by  $\tilde{b}r_3^2 + \Theta u_3^2 - u_3 = 0$ ; it consists of a left attracting branch  $\check{\mathcal{S}}_{0_3}^{a-}$  corresponding to  $u_3 \in [0, \frac{1}{2\Theta})$  and a right repelling branch  $\check{\mathcal{S}}_{0_3}^{a+}$  which is obtained for  $u_3 \in (\frac{1}{2\Theta}, \frac{1}{\Theta}]$ . The two branches are separated by the fold point  $A_{0_3}$ . Both branches are intersections of  $\mathcal{S}_{0_3}$  with the plane  $\{\delta_3 = 0\}$ . The geometry in chart  $K_3$  is summarised in Figure 10.

**Remark 16.** The manifolds  $\check{S}_{0_3}$  and  $\hat{S}_{0_3}$  correspond precisely to the critical manifolds  $\mathcal{S}_{00_1}$  and  $\mathcal{S}_{00_2}$  uncovered in regimes  $\mathcal{R}_1$  and  $\mathcal{R}_2$ , respectively. Hence, chart  $K_3$  covers the transition between those two regimes, as claimed.

Due to  $F_3(r_3, u_3, 0) = 0$ , the reduced flow with respect to  $\kappa$  in  $\{\delta_3 = 0\}$  is degenerate, in that it vanishes identically; hence,  $A_{0_3}$  is not a jump point in the classical sense of [14]. However, the equivalent of  $A_{0_3}$  in regime  $\mathcal{R}_1$ , denoted by  $A_{00_1}$  in Section 3.1, is, which allows for a description of the passage past  $A_{0_3}$  by recourse to  $\mathcal{R}_1$ ; see also the proof of Lemma 10 below.

**Remark 17.** Alternatively, one may note that, for  $\delta_3$  positive and small, the factor  $\left[ \tilde{\mu}(\delta_3 u_3 + 1) - \left( \delta_3^{\frac{1}{2}} u_3 + \tilde{d} r_3 \right) \right] = \tilde{\mu} - \tilde{d} r_3 - u_3 \delta_3^{\frac{1}{2}} \left( 1 - \tilde{\mu} \delta_3^{\frac{1}{2}} \right)$  in the definition of  $F_3$  is positive due to our choice of  $\mu$  and  $d$ , which implies  $\frac{\tilde{\mu}}{\tilde{d}} > (2\sqrt{\Theta\tilde{b}})^{-1}$ . Hence,  $r'_3 > 0$  for  $r_3 < (2\sqrt{\Theta\tilde{b}})^{-1}$ , i.e., the reduced flow in  $r_3$  is directed towards  $A_{0_3}$ : orbits follow the corresponding sheet  $\mathcal{S}_{0_3}^{a-}$  of  $S_{0_3}$  until they reach the fold curve  $\mathcal{F}_{0_3}^A$  and then jump away under the layer flow of Equation (43); recall Remark 7. (The corresponding touch-down point is not visible in chart  $K_3$ .)

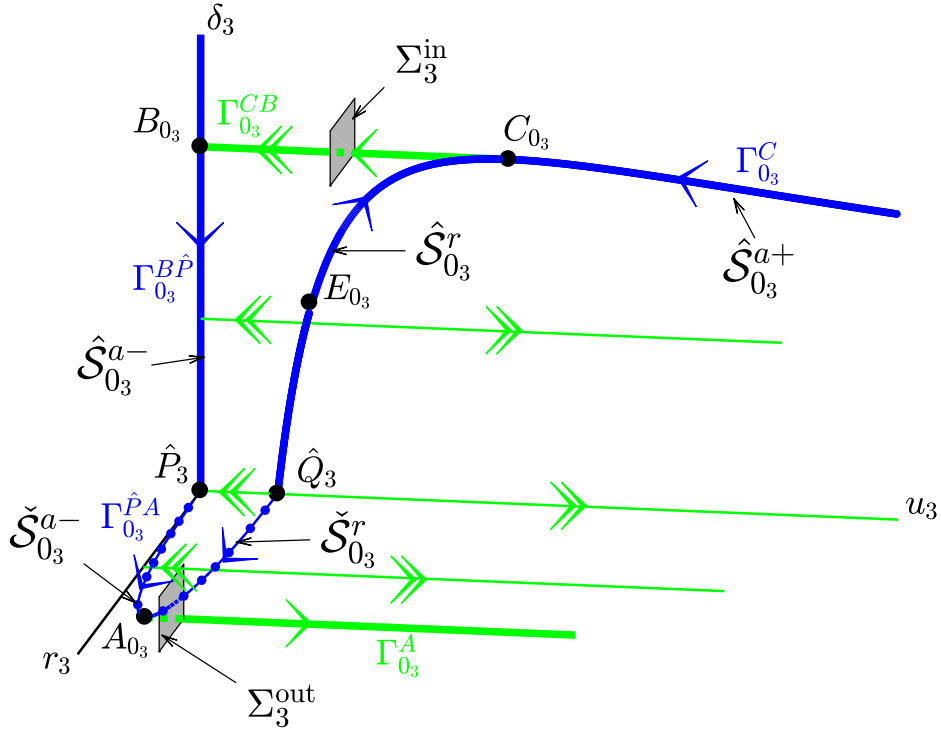


FIGURE 10. Geometry in  $\{r_3 = 0\}$  and  $\{\delta_3 = 0\}$ , for  $\kappa = 0$ , in chart  $K_3$ : reduced flow (solid blue), layer dynamics (solid green), and equilibrium  $E_{0_3}$ .

We conclude with the following result, the proof of which is analogous to that of Lemma 2:

**Lemma 4.** For  $r_3$  or  $\delta_3$  sufficiently small, the critical manifold  $\mathcal{S}_{0_3}$  that is defined by Equation (44) has the following properties:

- i. The manifold  $\mathcal{S}_{0_3} = \mathcal{S}_{0_3}^{a-} \cup \mathcal{F}_{0_3}^A \cup \mathcal{S}_{0_3}^r \cup \mathcal{F}_{0_3}^C \cup \mathcal{S}_{0_3}^{a+}$  is smooth.
- ii. The manifold  $\mathcal{S}_{0_3}$  has a folded structure; in particular, the branches  $\mathcal{S}_{0_3}^{a-}$  and  $\mathcal{S}_{0_3}^r$  are separated by the fold curve  $\mathcal{F}_{0_3}^A$ , while  $\mathcal{S}_{0_3}^r$  and  $\mathcal{S}_{0_3}^{a+}$  are separated by the fold curve  $\mathcal{F}_{0_3}^C$ .
- iii. The branches  $\mathcal{S}_{0_3}^{a-}$  and  $\mathcal{S}_{0_3}^{a+}$  are attracting under the layer flow of Equation (43), while the branch  $\mathcal{S}_{0_3}^r$  is repelling.

- iv. The restriction of  $\mathcal{S}_{0_3}^{a-}$ ,  $\mathcal{S}_{0_3}^r$ , and  $\mathcal{S}_{0_3}^{a+}$  to the invariant hyperplane  $\{r_3 = 0\}$  corresponds to  $\hat{\mathcal{S}}_{0_3}^{a-}$ ,  $\hat{\mathcal{S}}_{0_3}^r$ , and  $\hat{\mathcal{S}}_{0_3}^{a+}$ , respectively. Correspondingly, the fold curve  $F_{0_3}^C$  intersects  $\{r_3 = 0\}$  in the point  $C_{0_3}$ .
- v. In the invariant hyperplane  $\{\delta_3 = 0\}$ ,  $\mathcal{S}_{0_3}^{a-}$  and  $\mathcal{S}_{0_3}^r$  reduce to  $\check{\mathcal{S}}_{0_3}^{a-}$  and  $\check{\mathcal{S}}_{0_3}^r$ , respectively. The fold curve  $\mathcal{F}_{0_3}^A$  intersects  $\{\delta_3 = 0\}$  in the point  $A_{0_3}$ .

As in Section 4.3, we introduce two sections  $\Sigma_3^{\text{in}}$  and  $\Sigma_3^{\text{out}}$  for the flow of Equation (42) as

$$(48a) \quad \Sigma_3^{\text{in}} := \left\{ (r_3, u_3, \delta_3) \mid r_3 \in [r_*, r^*], u_3 - \frac{2}{\Theta} \in [u_*, u^*], \delta_3 - \frac{\Theta}{4} \in [\delta_*, \delta^*] \right\} \quad \text{and}$$

$$(48b) \quad \Sigma_3^{\text{out}} := \left\{ (r_3, \frac{1}{\Theta}, \delta_3) \mid r_3 - \frac{1}{2\sqrt{\Theta b}} \in [r_*, r^*], \delta_3 \in [\delta_*, \delta^*] \right\},$$

respectively, where  $r_*$ ,  $r^*$ ,  $u_*$ ,  $u^*$ ,  $\delta_*$ , and  $\delta^*$  are suitably chosen constants, as before. Here, we note that  $\Sigma_3^{\text{in}}$  is equivalent to the section  $\Sigma_1^{\text{out}}$  defined in (38) via the change-of-coordinates transformation in (40), while  $\Sigma_3^{\text{out}}$  is defined directly in chart  $K_3$ .

In summary, the segment  $\Gamma_{0_3}^C$  of the singular orbit follows the slow flow on  $\hat{\mathcal{S}}_{0_3}^{a+}$  to the fold point  $C_{0_3}$ ; the orbit  $\Gamma_{0_3}^{CB}$  represents the jump along the fast flow to the point  $B_{0_3}$ . The segment  $\Gamma_{0_3}^{B\hat{P}}$  then follows the slow flow on  $\hat{\mathcal{S}}_{0_3}^{a-}$  until it reaches the origin  $\hat{P}_3$ , continuing with the curve of equilibria  $\Gamma_{0_3}^{\hat{P}A}$  that corresponds to the segment of  $\check{\mathcal{S}}_{0_3}^{a-}$  between  $\hat{P}_3$  and the fold point  $A_{0_3}$ ; finally, the orbit jumps along the fast flow to the right for  $u_3$  large. We label the corresponding segment by  $\Gamma_{0_3}^A$ ; see Figure 10 for an illustration. The large- $u_3$  dynamics of Equation (42) is then naturally studied in chart  $K_4$ .

**4.6. Dynamics in chart  $K_4$ .** In chart  $K_4$ , the blow-up transformation defined by  $\bar{u}_1 = 1$  in Equation (39) is given as in (41). Substituting into Equation (31), dividing out a factor of  $\delta_4^2$ , and defining

$$F_4(r_4, \delta_4, \varepsilon_4) = F_1(r_4, \delta_4^2, \delta_4 \varepsilon_4) \delta_4^{-2} = \delta_4^{\frac{1}{2}} (\delta_4 + \mathcal{P} \varepsilon_4) \frac{(\delta_4 + \varepsilon_4)^2 + \Lambda r_4^2 \delta_4^2}{(\delta_4 + \varepsilon_4)(\delta_4 + \frac{\varepsilon_4}{c})} \\ \times \left[ \tilde{\mu} \varepsilon_4^{\frac{1}{2}} (\delta_4 + \varepsilon_4) - \left( \delta_4^{\frac{1}{2}} + \tilde{d} r_4 \varepsilon_4^{\frac{3}{2}} \right) \right],$$

we obtain the simplified system

$$(49a) \quad r_4' = \kappa r_4 F_4(r_4, \delta_4, \varepsilon_4),$$

$$(49b) \quad \delta_4' = \frac{1}{2} \delta_4 \left\{ \tilde{b} r_4^2 \varepsilon_4^2 (\delta_4 + \varepsilon_4)^2 + \Theta - [(\delta_4 + \varepsilon_4)^2 + \Lambda r_4^2 \delta_4^2] \right\} - \kappa \delta_4 F_4(r_4, \delta_4, \varepsilon_4),$$

$$(49c) \quad \varepsilon_4' = -\frac{1}{2} \varepsilon_4 \left\{ \tilde{b} r_4^2 \varepsilon_4^2 (\delta_4 + \varepsilon_4)^2 + \Theta - [(\delta_4 + \varepsilon_4)^2 + \Lambda r_4^2 \delta_4^2] \right\} - \kappa \varepsilon_4 F_4(r_4, \delta_4, \varepsilon_4),$$

which is a slow-fast system with singular perturbation parameter  $\kappa$ ; correspondingly, the variable  $r_4$  is slow, while  $\delta_4$  and  $\varepsilon_4$  are fast. Here, the prime again denotes differentiation with respect to a new independent variable.

**Remark 18.** The denominator  $(\delta_4 + \varepsilon_4)(\delta_4 + \frac{\varepsilon_4}{c})$  in  $F_4(r_4, \delta_4, \varepsilon_4)$  may be expected to render the limit as  $(\delta_4, \varepsilon_4) \rightarrow (0, 0)$  in (49) non-uniform. However,  $F_4$  again vanishes to the order  $\mathcal{O}(2)$  at  $(\delta_4, \varepsilon_4) = (0, 0)$ ; recall Remark 14.

Setting  $\kappa = 0$  in (49), we obtain the layer problem

$$(50a) \quad r_4' = 0,$$

$$(50b) \quad \delta_4' = \frac{1}{2} \delta_4 \left\{ \tilde{b} r_4^2 \varepsilon_4^2 (\delta_4 + \varepsilon_4)^2 + \Theta - [(\delta_4 + \varepsilon_4)^2 + \Lambda r_4^2 \delta_4^2] \right\},$$

$$(50c) \quad \varepsilon_4' = -\frac{1}{2} \varepsilon_4 \left\{ \tilde{b} r_4^2 \varepsilon_4^2 (\delta_4 + \varepsilon_4)^2 + \Theta - [(\delta_4 + \varepsilon_4)^2 + \Lambda r_4^2 \delta_4^2] \right\}.$$



The corresponding critical manifold  $\mathcal{S}_{0_4}$  is the hypersurface in  $(r_4, \delta_4, \varepsilon_4)$ -space that is defined by

$$(51) \quad \tilde{b}r_4^2\varepsilon_4^2(\delta_4 + \varepsilon_4)^2 + \Theta - [(\delta_4 + \varepsilon_4)^2 + \Lambda r_4^2\delta_4^2] = 0;$$

an additional line of equilibria is found for  $\delta_4 = 0 = \varepsilon_4$ , i.e., on the  $r_4$ -axis.

**Remark 19.** Since  $\delta_4$  and  $\varepsilon_4$  are fast variables outside of a neighbourhood of  $\mathcal{S}_{0_4}$ , Equation (49) is not a slow-fast system in standard form; details can be found in [13].

We consider the flow of Equation (50) in the invariant plane  $\{\delta_4 = 0\}$ , which is governed by

$$(52a) \quad r_4' = 0,$$

$$(52b) \quad \varepsilon_4' = -\frac{1}{2}\varepsilon_4(\tilde{b}r_4^2\varepsilon_4^4 + \Theta - \varepsilon_4^2).$$

The corresponding critical manifold is defined by

$$\tilde{b}r_4^2\varepsilon_4^4 + \Theta - \varepsilon_4^2 = 0;$$

it consists of a lower repelling branch  $\check{\mathcal{S}}_{0_4}^r$  corresponding to  $\varepsilon_4 \in [\sqrt{\Theta}, \sqrt{2\Theta})$  and an upper attracting branch  $\check{\mathcal{S}}_{0_4}^{a-}$  with  $\varepsilon_4 \in (\sqrt{2\Theta}, \infty)$ , which are separated by the fold point  $A_{0_4}$ . We denote the line of additional equilibria on the  $r_4$ -axis by  $\check{\ell}_{0_4}$ ; here, we emphasise that  $\check{\ell}_{0_4}$  is attracting in  $\{\delta_4 = 0\}$ . All three branches are found in the intersection of  $\mathcal{S}_{0_4}$  with the plane  $\{\delta_4 = 0\}$ . Orbits follow the slow manifold  $\check{\mathcal{S}}_{0_4}^{a-}$  until they reach the fold point at  $A_{0_4}$ , where they jump forward to the point  $\check{P}_4 : \left(\frac{1}{2\sqrt{\Theta\tilde{b}}}, 0, 0\right) \in \check{\ell}_{0_4}$ .

In the invariant plane  $\{\varepsilon_4 = 0\}$ , Equation (50) reduces to

$$(53a) \quad r_4' = -\kappa r_4\delta_4^2(1 + \Lambda r_4^2),$$

$$(53b) \quad \delta_4' = \frac{1}{2}\delta_4[\Theta - \delta_4^2(1 + \Lambda r_4^2)] + \kappa\delta_4^3(1 + \Lambda r_4^2),$$

as  $F_4(r_4, \delta_4, 0) = -\delta_4^2(1 + \Lambda r_4^2)$  then. The corresponding layer problem is obtained for  $\kappa = 0$ :

$$(54a) \quad r_4' = 0,$$

$$(54b) \quad \delta_4' = \frac{1}{2}\delta_4[\Theta - \delta_4^2(1 + \Lambda r_4^2)],$$

which implies that the critical manifold satisfies  $\Theta - \delta_4^2(1 + \Lambda r_4^2) = 0$ . That manifold consists of an attracting branch  $\check{\mathcal{S}}_{0_4}^{a+}$ , which intersects the  $\delta_4$ -axis in the point  $\check{Q}_4 = (0, \sqrt{\Theta}, 0)$ ; the line of equilibria on the  $r_4$ -axis, denoted again by  $\check{\ell}_{0_4}$ , is repelling in  $\{\varepsilon_4 = 0\}$ . Orbits starting close to  $\check{P}_4 \in \check{\ell}_{0_4}$  leave along the unstable manifold thereof and jump to the point  $D_{0_4} : \left(\frac{1}{2\sqrt{\Theta\tilde{b}}}, \frac{2\Theta\sqrt{\tilde{b}}}{\sqrt{4\Theta\tilde{b} + \Lambda}}, 0\right)$  in  $\check{\mathcal{S}}_{0_4}^{a+}$ ; then, they follow the slow manifold  $\check{\mathcal{S}}_{0_4}^{a+}$  until they reach the point  $\check{Q}_4$ . An illustration of the resulting geometry can be found in Figure 11.

Similarly, in the invariant plane  $\{r_4 = 0\}$ , the flow of Equation (50) is governed by

$$(55a) \quad \delta_4' = \frac{1}{2}\delta_4[\Theta - (\delta_4 + \varepsilon_4)^2] - \kappa\delta_4 F_4(0, \delta_4, \varepsilon_4),$$

$$(55b) \quad \varepsilon_4' = -\frac{1}{2}\varepsilon_4[\Theta - (\delta_4 + \varepsilon_4)^2] - \kappa\varepsilon_4 F_4(0, \delta_4, \varepsilon_4),$$

where

$$F_4(0, \delta_4, \varepsilon_4) = \delta_4^{\frac{1}{2}}(\delta_4 + \mathcal{P}\varepsilon_4)\frac{\delta_4 + \varepsilon_4}{\delta_4 + \frac{\varepsilon_4}{c}}\left[\tilde{\mu}\varepsilon_4^{\frac{1}{2}}(\delta_4 + \varepsilon_4) - \delta_4^{\frac{1}{2}}\right].$$



- i. The manifold  $\mathcal{S}_{0_4} = \mathcal{S}_{0_4}^{a-} \cup \mathcal{F}_{0_4}^A \cup \mathcal{S}_{0_4}^r \cup \mathcal{F}_{0_4}^C \cup \mathcal{S}_{0_4}^{a+}$  is smooth away from the line  $\check{\ell}_{0_4}$ .
- ii. The manifold  $\mathcal{S}_{0_4}$  has a folded structure; in particular, the branches  $\mathcal{S}_{0_4}^{a-}$  and  $\mathcal{S}_{0_4}^r$  are separated by the fold curve  $\mathcal{F}_{0_4}^A$ , while  $\mathcal{S}_{0_4}^r$  and  $\mathcal{S}_{0_4}^{a+}$  are separated by the fold curve  $\mathcal{F}_{0_4}^C$ .
- iii. The branches  $\mathcal{S}_{0_4}^{a-}$  and  $\mathcal{S}_{0_4}^{a+}$  are attracting under the layer flow of Equation (50), while the branch  $\mathcal{S}_{0_4}^r$  is repelling.
- iv. The restriction of  $\mathcal{S}_{0_4}^r$  and  $\mathcal{S}_{0_4}^{a+}$  to the invariant hyperplane  $\{r_4 = 0\}$  corresponds to  $\hat{\mathcal{S}}_{0_4}^r$  and  $\hat{\mathcal{S}}_{0_4}^{a+}$ , respectively. Correspondingly, the fold curve  $\mathcal{F}_{0_4}^C$  intersects  $\{r_4 = 0\}$  in the point  $C_{0_4}$ .
- v. In the invariant hyperplane  $\{\delta_4 = 0\}$ ,  $\mathcal{S}_{0_4}^{a-}$  and  $\mathcal{S}_{0_4}^r$  reduce to  $\check{\mathcal{S}}_{0_4}^{a-}$  and  $\check{\mathcal{S}}_{0_4}^r$ , respectively. The fold curve  $\mathcal{F}_{0_4}^A$  intersects  $\{\delta_4 = 0\}$  in the point  $A_{0_4}$ .
- vi. The restriction of  $\mathcal{S}_{0_4}^{a+}$  to the invariant hyperplane  $\{\varepsilon_4 = 0\}$  corresponds to  $\check{\mathcal{S}}_{0_4}^{a+}$ .
- vii. The line  $\check{\ell}_{0_4}$  consists of saddle-type equilibria for Equation (49), with 1-dimensional stable manifold in the hyperplane  $\{\delta_4 = 0\}$  and 1-dimensional unstable manifold in the hyperplane  $\{\varepsilon_4 = 0\}$ .

Again, we define two sections  $\Sigma_4^{\text{in}}$  and  $\Sigma_4^{\text{out}}$  for the flow of Equation (49); here, the former is obtained as the image of the section  $\Sigma_3^{\text{out}}$  from chart  $K_3$  under the transformation  $\mathcal{K}_{34}$  defined in Lemma 3, while the latter is the image of the section  $\Sigma_1^{\text{in}}$  from chart  $K_1$  in  $K_4$  under the transformation

$$\mathcal{K}_{14} : (\rho_1, u_1, \varepsilon_1) \mapsto (r_4, \delta_4^2, \delta_4 \varepsilon_4).$$

Hence,  $\Sigma_4^{\text{in}}$  and  $\Sigma_4^{\text{out}}$  can be represented as

$$(57a) \quad \Sigma_4^{\text{in}} := \left\{ (r_4, \delta_4, \sqrt{\Theta}) \mid r_4 - \frac{1}{2\sqrt{\Theta b}} \in [r_*, r^*], \delta_4 \in [\delta_*, \delta^*] \right\} \quad \text{and}$$

$$(57b) \quad \Sigma_4^{\text{out}} := \left\{ (r_4, \frac{\sqrt{\Theta}}{2}, \varepsilon_4) \mid r_4 - \frac{1}{2\sqrt{\Theta b}} \in [r_*, r^*], \varepsilon_4 \in [\varepsilon_*, \varepsilon^*] \right\},$$

where the constants  $r_*$ ,  $r^*$ ,  $\delta_*$ ,  $\delta^*$ ,  $\varepsilon_*$ , and  $\varepsilon^*$  are again suitably chosen.

**Remark 21.** We emphasise that our blow-up of the non-hyperbolic line  $\check{\ell}_{0_1}$  from chart  $K_1$  to a cylinder has resulted in a gain of hyperbolicity; in particular, the line  $\check{\ell}_{0_4}$  in  $K_4$  is of saddle type, by item *vii* above.

To summarise, the segment  $\Gamma_{0_4}^{A\check{P}}$  of the singular cycle is initiated close to the fold point  $A_{0_4}$  and is attracted to  $\check{\mathcal{S}}_{0_4}^{a-}$ , where it jumps forward along the fast flow to the point  $\check{P}_4$ ; the orbit  $\Gamma_{0_4}^{\check{P}D}$  then leaves along the unstable manifold thereof and is attracted by  $\check{\mathcal{S}}_{0_4}^{a+}$ , connecting to the point  $D_{0_4}$ . The orbit  $\Gamma_{0_4}^{D\check{Q}}$  follows the slow flow on  $\check{\mathcal{S}}_{0_4}^{a+}$  to the point  $\check{Q}_4$  and continues as the orbit  $\Gamma_{0_4}^{\check{Q}C}$  along the slow flow on  $\hat{\mathcal{S}}_{0_4}^{a+}$  until it reaches the point  $C_{0_4}$ , where the orbit  $\Gamma_{0_4}^C$  represents the jump back which is, however, not visible in chart  $K_4$ , but is discussed in  $K_3$  already. (Clearly, the manifolds  $\check{\mathcal{S}}_{0_3}^{a-}$ ,  $\check{\mathcal{S}}_{0_3}^r$ ,  $\hat{\mathcal{S}}_{0_3}^{a+}$ , and  $\hat{\mathcal{S}}_{0_3}^r$  defined in chart  $K_3$  correspond to  $\check{\mathcal{S}}_{0_4}^{a-}$ ,  $\check{\mathcal{S}}_{0_4}^r$ ,  $\hat{\mathcal{S}}_{0_4}^{a+}$ , and  $\hat{\mathcal{S}}_{0_4}^r$ , respectively.) The geometry in the planes  $\{\delta_4 = 0\}$ ,  $\{\varepsilon_4 = 0\}$ , and  $\{r_4 = 0\}$  in chart  $K_4$  is illustrated in Figure 11.

**4.7. Global geometry in blown-up space.** We now summarise the global geometry of the blown-up space, which we denote as  $\bar{M}_\kappa$ , with  $\kappa \in [0, \kappa_0]$ . The above analysis implies that  $\bar{M}_\kappa$  contains the sphere  $M_U$  and the cylinder  $M_R$ , which are obtained by the blow-up transformation in (24) at the origin  $Q$  in  $(R, U, \varepsilon)$ -space and the blow-up in (39) of the non-hyperbolic line  $\check{\ell}_{0_1}$  in chart  $K_1$  of the former, respectively; see Figure 13. We recall that the vector field  $X_\kappa$  corresponding to Equation (6), which is defined on  $\mathbb{R}^3$ , induces a blown-up vector field  $\bar{X}_\kappa$  on the blown-up space  $\bar{M}_\kappa$ ; blow-up resolves the degeneracy of the critical manifold  $\mathcal{S}_0$  – with  $\kappa$  as the singular perturbation parameter – at  $\varepsilon = 0$ . In particular, the equation  $\varepsilon' = 0$  implies an invariant foliation of  $\bar{M}_\kappa$  in  $\varepsilon$ , with the singular leaf defined by  $\varepsilon = 0$  corresponding to the union of the sphere  $M_U$ , the cylinder  $M_R$ , and the plane  $\{\bar{\varepsilon} = 0\}$ . It follows that, for  $\kappa = 0$ , the restriction of  $\bar{X}_0$  to that singular leaf represents the double singular limit of  $(\kappa, \varepsilon) \rightarrow (0, 0)$ ,

which has now been resolved in the blown-up space  $\bar{M}_0$ . The following results follow immediately from our discussion in Section 4; see also [13, Theorem 4.5].

**Lemma 6.** *The critical manifold of system (23), for  $\kappa = 0$ , in the blown-up space  $\bar{M}_0$  is defined as*

$$\bar{S}_0 = \bar{S}_0^{a-} \cup \bar{F}_0^A \cup \bar{S}_0^r \cup \bar{F}_0^C \cup \bar{S}_0^{a+};$$

here, the branches  $\bar{S}_0^{a-}$  and  $\bar{S}_0^{a+}$  are attracting under the layer flow that is induced by Equation (8) after blow-up, while the branch  $\bar{S}_0^r$  is repelling. Moreover,  $\bar{S}_0^{a-}$  and  $\bar{S}_0^{a+}$  are separated by the fold curve  $\bar{F}_0^A$ , while  $\bar{S}_0^r$  and  $\bar{S}_0^{a+}$  are separated by the fold curve  $\bar{F}_0^C$ .

(We recall that, by Remark 13, any object  $\square_{\kappa\varepsilon}$  is written as  $\square_\kappa$  after blow-up.)

Lemma 6 implies that a unique singular cycle  $\bar{\Gamma}_{00}$  can now be defined in the blown-up space  $\bar{M}_\kappa$  due to the improved transversality and hyperbolicity properties of the flow therein; for clarity, we label the corresponding persistent cycle in blown-up space by  $\bar{\Gamma}_{\kappa\varepsilon}$  which, for  $(\kappa, \varepsilon) \rightarrow (0, 0)$ , yields the singular cycle  $\bar{\Gamma}_{00}$ .

**Lemma 7.** *The singular cycle  $\bar{\Gamma}_{00}$  is defined by*

$$\bar{\Gamma}_{00} = \bar{\Gamma}_{00}^{A\hat{P}} \cup \bar{\Gamma}_{00}^{\hat{P}D} \cup \bar{\Gamma}_{00}^{D\check{Q}} \cup \bar{\Gamma}_{00}^{\check{Q}C} \cup \bar{\Gamma}_{00}^{CB} \cup \bar{\Gamma}_{00}^{B\hat{P}} \cup \bar{\Gamma}_{00}^{\hat{P}A}.$$

Here, the heteroclinic connection  $\bar{\Gamma}_{00}^{A\hat{P}}$  is located on the cylinder  $M_R$  and represents the fast jump from the point  $\bar{A}_0$  to the point  $\hat{P} \in \bar{S}_0^r$ ; the orbit  $\bar{\Gamma}_{00}^{\hat{P}D}$  lies in the plane  $\{\bar{\varepsilon} = 0\}$ , connecting  $\hat{P}$  to the point  $\bar{D}_0 \in \bar{S}_0^{a+}$ . Finally,  $\bar{\Gamma}_{00}^{D\check{Q}}$  represents the transition on  $\bar{S}_0^{a+}$  from  $\bar{D}_0$  to the point  $\check{Q}$ . On the sphere  $M_U$ , the segment  $\bar{\Gamma}_{00}^{\check{Q}C}$  on  $\bar{S}_0^{a+}$  connects the point  $\check{Q}$  to the fold point at  $\bar{C}_0$ ;  $\bar{\Gamma}_{00}^{CB}$  denotes the heteroclinic connection from  $\bar{C}_0$  to the point  $\bar{B}_0 \in \bar{S}_0^{a-}$ , followed by the orbit  $\bar{\Gamma}_{00}^{B\hat{P}}$  from  $\bar{B}_0$  to the point  $\hat{P}$ . The final segment  $\bar{\Gamma}_{00}^{\hat{P}A}$  is located on the cylinder  $M_R$ , and denotes the connection on  $\bar{S}_0^{a-}$  from  $\hat{P}$  to the fold point at  $\bar{A}_0$ .

An illustration of  $\bar{\Gamma}_{00}$  can be found in Figure 13; here, the reduced flow for  $(\kappa, \varepsilon) = (0, 0)$  is shown in blue, as are the corresponding critical manifolds, while the layer dynamics is illustrated in green. We emphasise that chart  $K_2$  is not required for our construction, strictly speaking, as the relevant portions of  $\bar{\Gamma}_{00}$  can be obtained in either chart  $K_1$  or  $K_3$ ; recall Figures 9 and 10, respectively.

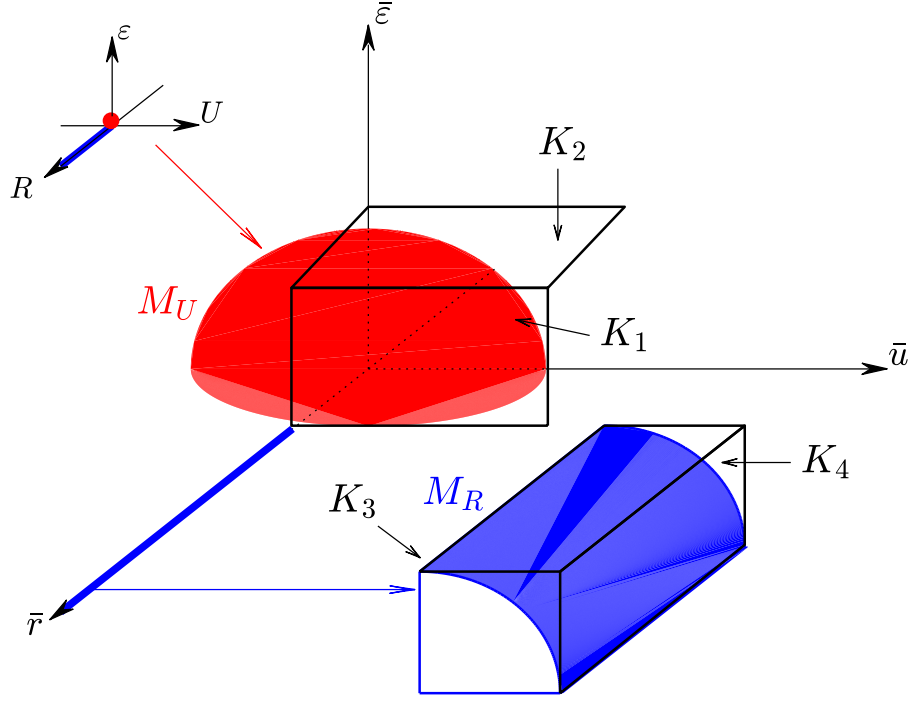


FIGURE 12. The charts  $K_i$  ( $i = 1, \dots, 4$ ) in the blown-up space  $\bar{M}_\kappa$ .

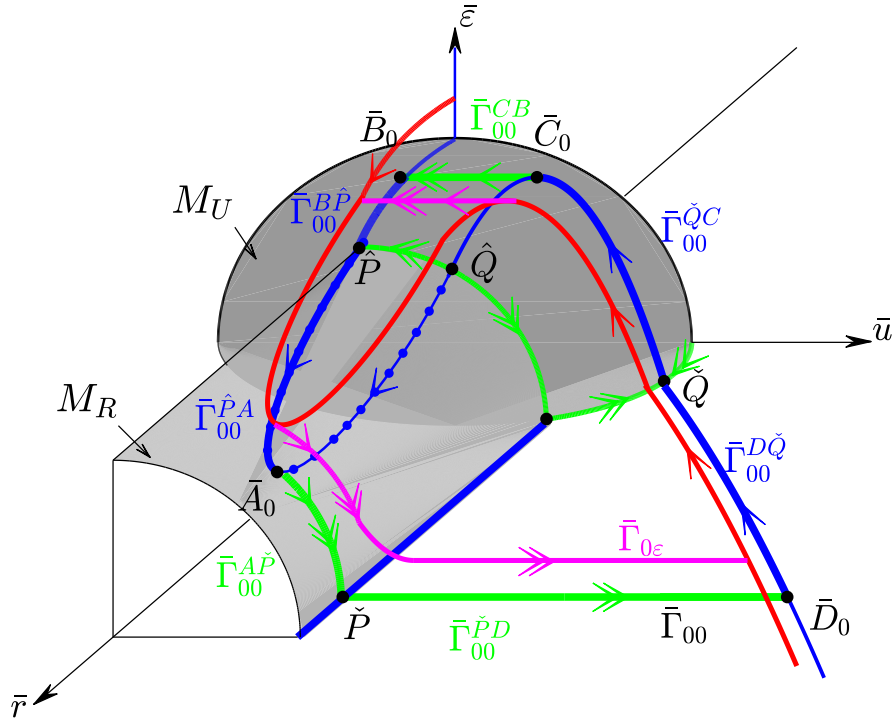


FIGURE 13. Geometry of the blown-up space  $\bar{M}_0$ : singular cycle  $\bar{\Gamma}_{00}$  (solid blue; solid green) and singular cycle  $\bar{\Gamma}_{0\varepsilon}$  (solid red; solid pink).

Next, we have the following result on the persistence of  $\bar{\Gamma}_{00}$ , for  $\varepsilon$  positive and sufficiently small:

**Lemma 8.** *For  $\varepsilon \in (0, \varepsilon_0]$ , with  $\varepsilon_0$  positive and sufficiently small, there exists a singular cycle  $\bar{\Gamma}_{0\varepsilon}$  which follows the slow flow on  $\bar{\mathcal{S}}_0^{a-}$  and  $\bar{\mathcal{S}}_0^{a+}$ , with jumps at the fold curves  $\bar{\mathcal{F}}_0^A$  and  $\bar{\mathcal{F}}_0^C$ ; that cycle limits on  $\bar{\Gamma}_{00}$  as  $\varepsilon \rightarrow 0$ .*

The orbit  $\bar{\Gamma}_{0\varepsilon}$  is again illustrated in Figure 13; here, we emphasise that  $\bar{\Gamma}_{0\varepsilon}$  is obtained as a perturbation off  $\bar{\Gamma}_{00}$  for  $\varepsilon \in (0, \varepsilon_0]$  and  $\kappa = 0$ . (The corresponding reduced flow is shown in red, while the layer dynamics is illustrated in pink.)

**Remark 22.** Intuitively, blow-up desingularises the limit as  $\varepsilon \rightarrow 0$  in our definition of the critical manifold  $\mathcal{S}_{0\varepsilon}$  for Equation (9), in that the non-uniform collapse of that manifold onto the degenerate manifold  $\mathcal{S}_{00}$  has been prevented; in particular, the folded structure of  $\mathcal{S}_{0\varepsilon}$  remains visible for  $\varepsilon = 0$  after blow-up.

Finally, and in analogy to Theorem 4.6 in [13], we can conclude that, for  $\kappa \in (0, \kappa_0]$ , the blown-up vector field  $\bar{X}_\kappa$  admits smooth slow manifolds  $\bar{\mathcal{S}}_\kappa^{a-}$ ,  $\bar{\mathcal{S}}_\kappa^r$ , and  $\bar{\mathcal{S}}_\kappa^{a+}$  away from the fold curves  $\bar{\mathcal{F}}_0^A$  and  $\bar{\mathcal{F}}_0^C$ ; in accordance with standard practice [23], we assume that these manifolds are extended beyond  $\bar{\mathcal{F}}_0^A$  and  $\bar{\mathcal{F}}_0^C$  by the flow corresponding to  $\bar{X}_\kappa$ .

## 5. POINCARÉ MAP AND EXISTENCE

To prove the persistence of the singular cycle  $\bar{\Gamma}_{00}$  for  $\kappa$  and  $\varepsilon$  sufficiently small, we construct a Poincaré map in the neighborhood of  $\bar{\Gamma}_{00}$  which is obtained through the concatenation of three transition maps  $\Pi_i$  ( $i = 1, 3, 4$ ) between specific sections for the flow in the blown-up space  $\bar{M}_\kappa$ ; see Figure 14.

- i. The transition map  $\Pi_1 : \Sigma_1 \rightarrow \Sigma_3$  is initialised in the section  $\Sigma_1$ ; the corresponding flow is attracted to the slow manifold  $\bar{\mathcal{S}}_\kappa^{a+}$ , which it follows up to the non-hyperbolic fold curve  $\bar{\mathcal{F}}_0^C$ , where it jumps, remaining close to the heteroclinic connection  $\bar{\Gamma}_{00}^{CB}$  to reach a section  $\Sigma_3$ .
- ii. The transition map  $\Pi_3 : \Sigma_3 \rightarrow \Sigma_4$  is initialised in the section  $\Sigma_3$ ; the corresponding flow is attracted to the slow manifold  $\bar{\mathcal{S}}_\kappa^{a-}$ , which it follows up to the non-hyperbolic fold curve  $\bar{\mathcal{F}}_0^A$ . It then jumps, remaining close to the heteroclinic connection  $\bar{\Gamma}_{00}^{A\bar{P}}$ , to reach a section  $\Sigma_4$ .
- iii. The transition map  $\Pi_4 : \Sigma_4 \rightarrow \Sigma_1$  is initialised in the section  $\Sigma_4$ ; the corresponding flow then remains close to the heteroclinic connection  $\bar{\Gamma}_{00}^{A\bar{P}}$ , passing near the hyperbolic line  $\bar{\ell}_0$  and the singular heteroclinic  $\bar{\Gamma}_{00}^{\bar{P}D}$  to reach a section  $\Sigma_1$ .

The Poincaré map  $\Pi : \Sigma_1 \rightarrow \Sigma_1$ , which is a global return map, is now defined as the composition  $\Pi = \Pi_4 \circ \Pi_3 \circ \Pi_1$ . Here, we note that the maps  $\Pi_i$  ( $i = 1, 3, 4$ ) are constructed in charts  $K_i$ , respectively; details can be found in the following subsections.

**Remark 23.** The sections  $\Sigma_1$ ,  $\Sigma_3$ , and  $\Sigma_4$  are defined to be transversal to the heteroclinic orbits  $\bar{\Gamma}_{00}^{\bar{P}D}$ ,  $\bar{\Gamma}_{00}^{CB}$ , and  $\bar{\Gamma}_{00}^{A\bar{P}}$ , respectively; see again Figure 14.

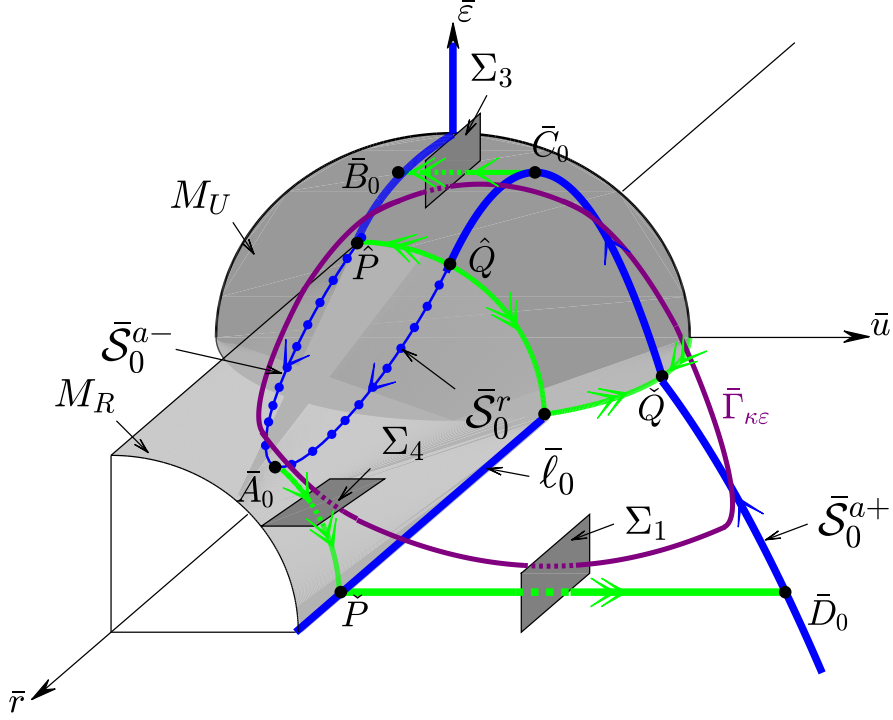


FIGURE 14. Illustration of the Poincaré map  $\Pi$ : sections  $\Sigma_1$ ,  $\Sigma_3$ , and  $\Sigma_4$  (shaded dark grey); singular cycle  $\bar{\Gamma}_{00}$  (solid blue; solid green); sample periodic orbit  $\bar{\Gamma}_{\kappa\epsilon}$  (solid purple).

**5.1. Transition map  $\Pi_1$ .** The transition map  $\Pi_1$  is constructed in chart  $K_1$  as a mapping between the sections  $\Sigma_1$  and  $\Sigma_3$ , which correspond to  $\Sigma_1^{\text{in}}$  and  $\Sigma_1^{\text{out}}$ , respectively; recall Equation (38). We note that, since  $\epsilon = \rho_1^2 \epsilon_1$  in  $K_1$ , invariant leaves of the form  $\{\epsilon \equiv \text{constant}\}$  satisfy  $\epsilon_1 \approx 4\Theta\tilde{b}\epsilon$  in  $\Sigma_1^{\text{in}}$  and  $\rho_1 \approx \frac{2}{\sqrt{\Theta}}\sqrt{\epsilon}$  in  $\Sigma_1^{\text{out}}$ .

**Lemma 9.** *For  $(\kappa, \epsilon) \in (0, \kappa_0] \times (0, \epsilon_0]$  with  $\kappa_0$  and  $\epsilon_0$  positive and sufficiently small, the transition map  $\Pi_1$  is well-defined. Moreover, the restriction of  $\Pi_1$  to the leaf  $\{\epsilon \equiv \text{constant}\}$  is a contraction (in  $\rho_1$ ) with contraction rate  $\mathcal{O}(e^{-\nu/\kappa})$ , where  $\nu$  is a positive constant.*

*Proof.* The passage past a regular fold point is studied in detail in [14]; in particular, it follows from the analysis therein that orbits initiated in  $\Sigma_1^{\text{in}}$  are attracted by the extended slow manifold  $\bar{S}_{\kappa}^{a+}$  at a contraction rate of the order  $\mathcal{O}(e^{-\nu/\kappa})$ , while the distance between the intersection of that extended manifold with  $\Sigma_1^{\text{out}}$  and the singular cycle  $\bar{\Gamma}_{00}$  is of the order  $\mathcal{O}(\kappa^{2/3})$ .  $\square$

**Remark 24.** While our approximation of the transition map  $\Pi_1$  is performed in chart  $K_1$ , the dynamics in that chart can also be recovered in regime  $\mathcal{R}_2$ . Hence, the results of [14] on passage past a singularly perturbed planar fold can be applied to Equation (18). For a more detailed analysis of chart  $K_1$ , we refer to [23], where general folds in  $\mathbb{R}^3$  are studied. Finally, we remark that passage past the point  $\check{Q}_1$  can be studied in terms of well-adapted normal forms that are derived in [1].

**5.2. Transition map  $\Pi_3$ .** The transition map  $\Pi_3$  is constructed in chart  $K_3$  as a mapping between the sections  $\Sigma_3$  and  $\Sigma_4$ . Here, we recall that these sections correspond to  $\Sigma_3^{\text{in}}$  and  $\Sigma_3^{\text{out}}$ , respectively; cf. Equation (48). Due to  $\epsilon = r_3^2 \delta_3$  in  $K_3$ , leaves with  $\{\epsilon \equiv \text{constant}\}$  satisfy  $r_3 \approx \sqrt{\frac{4}{\Theta}\epsilon}$  in  $\Sigma_3^{\text{in}}$  and  $\delta_3 \approx 4\Theta\tilde{b}\epsilon$  in  $\Sigma_3^{\text{out}}$ .

We have the following result, the proof of which is analogous to that of Lemma 9:

**Lemma 10.** For  $(\kappa, \varepsilon) \in (0, \kappa_0] \times (0, \varepsilon_0]$  with  $\kappa_0$  and  $\varepsilon_0$  positive and sufficiently small, the transition map  $\Pi_3$  is well-defined. Moreover, the restriction of  $\Pi_3$  to the leaf  $\{\varepsilon \equiv \text{constant}\}$  is a contraction (in  $r_3$ ) with contraction rate  $\mathcal{O}(e^{-\nu/\kappa})$ , where  $\nu$  is a positive constant.

**Remark 25.** Again, the map  $\Pi_3$  can alternatively be approximated in regime  $\mathcal{R}_1$ , i.e., by reference to Equation (14), to which the results of [14] apply. A more detailed analysis of chart  $K_3$  can be based on [23].

**5.3. Transition map  $\Pi_4$ .** The transition map  $\Pi_4$  is constructed in chart  $K_4$  as a mapping between the sections  $\Sigma_4$  and  $\Sigma_1$  which correspond to  $\Sigma_4^{\text{in}}$  and  $\Sigma_4^{\text{out}}$ , respectively, as defined in Equation (57).

**Lemma 11.** For  $(\kappa, \varepsilon) \in (0, \kappa_0] \times (0, \varepsilon_0]$  with  $\kappa_0$  and  $\varepsilon_0$  positive and sufficiently small, the transition map  $\Pi_4 : \Sigma_4 \rightarrow \Sigma_1$ ,  $(r_4^{\text{in}}, \delta_4^{\text{in}}, \sqrt{\Theta}) \mapsto (r_4^{\text{out}}, \frac{\sqrt{\Theta}}{2}, \varepsilon_4^{\text{out}})$  is well-defined; here,  $\delta_4^{\text{in}} \approx 4\sqrt{\Theta}\tilde{b}\varepsilon$  and  $\varepsilon_4^{\text{out}} \approx 8\sqrt{\Theta}\tilde{b}\varepsilon$ . In particular, as the restriction of  $\Pi_4$  to a leaf  $\{\varepsilon \equiv \text{constant}\}$  satisfies

$$r_4^{\text{out}} = r_4^{\text{in}} + \mathcal{O}(\kappa)$$

with  $r_4^{\text{in}} \approx \frac{1}{2\sqrt{\Theta}\tilde{b}}$ , the map  $\Pi_4$  is at mostly weakly expanding.

*Proof.* Recall the governing equations in chart  $K_4$ , as given in Equation (49), as well as the definition of  $F_4(r_4, \delta_4, \varepsilon_4)$  therein; dividing out the factor  $\frac{1}{2}\{\tilde{b}r_4^2\varepsilon_4^2(\delta_4 + \varepsilon_4)^2 + \Theta - [(\delta_4 + \varepsilon_4)^2 + \Lambda r_4^2\delta_4^2]\}$  from the right-hand sides in (49) and factoring out  $\delta_4^{\frac{1}{2}}$  from  $F_4$ , we obtain the new system

$$(58a) \quad r_4' = \kappa r_4 \delta_4^{\frac{1}{2}} \tilde{F}_4(r_4, \delta_4, \varepsilon_4),$$

$$(58b) \quad \delta_4' = \delta_4 - \kappa \delta_4^{\frac{3}{2}} \tilde{F}_4(r_4, \delta_4, \varepsilon_4),$$

$$(58c) \quad \varepsilon_4' = -\varepsilon_4 - \kappa \delta_4^{\frac{1}{2}} \varepsilon_4 \tilde{F}_4(r_4, \delta_4, \varepsilon_4),$$

where  $\tilde{F}_4(r_4, \delta_4, \varepsilon_4)$  is smooth and  $\mathcal{O}(1)$ . Equation (58) is again a slow-fast system in standard form; considering the layer problem

$$\begin{aligned} r_4' &= 0, \\ \delta_4' &= \delta_4, \\ \varepsilon_4' &= -\varepsilon_4, \end{aligned}$$

we can estimate the transition time  $T_4$  in  $\{\varepsilon \equiv \text{constant}\}$  under  $\Pi_4$ : since  $\delta_4 \approx 4\sqrt{\Theta}\tilde{b}\varepsilon$  in  $\Sigma_4^{\text{in}}$  and  $\varepsilon_4 \approx 8\sqrt{\Theta}\tilde{b}\varepsilon$  in  $\Sigma_4^{\text{out}}$  due to  $\varepsilon = r_4^2\delta_4\varepsilon_4$  in chart  $K_4$ , it follows that  $T_4 = \mathcal{O}(-\ln \varepsilon)$ . Finally, since  $r_4\delta_4^{\frac{1}{2}} = \sqrt{\frac{\varepsilon}{\varepsilon_4}}$  and  $\varepsilon_4 \approx \sqrt{\Theta}e^{-t}$ , we may write (58a) as  $r_4' = \kappa\sqrt{\varepsilon}e^{t/2} \cdot \mathcal{O}(1)$ , from which the statement of the lemma follows.  $\square$

**5.4. Proof of Theorem 1.** To conclude the proof of Theorem 1, we combine the above asymptotics of the transition maps  $\Pi_i$  ( $i = 1, 3, 4$ ) into the Poincaré map  $\Pi$ , which yields

**Theorem 2.** For  $\varepsilon \in (0, \varepsilon_0]$ , with  $\varepsilon_0$  positive and sufficiently small, there exists  $\kappa_0 = \kappa_0(\varepsilon_0)$  such that the blown-up vector field  $\bar{X}_\kappa$  admits a unique family of attracting periodic orbits  $\bar{\Gamma}_{\kappa\varepsilon}$  for  $\kappa \in (0, \kappa_0]$ . That family tends to  $\bar{\Gamma}_{0\varepsilon}$  as  $\kappa \rightarrow 0$  uniformly for  $\varepsilon \in (0, \varepsilon_0]$ , and converges to the singular cycle  $\bar{\Gamma}_{00}$  as  $(\kappa, \varepsilon) \rightarrow (0, 0)$ .

*Proof.* The proof follows from a combination of Lemmas 9, 10, and 11, in conjunction with the contraction mapping theorem. Specifically, since  $\rho_1 = R = r_3$ , the restriction of the maps  $\Pi_1$  and  $\Pi_3$  to leaves with  $\{\varepsilon \equiv \text{constant}\}$  is contracting in  $R$ , while  $\Pi_4$  is at most weakly expanding in  $R(= r_4)$ .  $\square$



An indicative illustration of the orbit  $\bar{\Gamma}_{\kappa\varepsilon}$ , for  $(\kappa, \varepsilon)$  positive and fixed, can be found in Figure 14.

Theorem 1 is a direct consequence of Theorem 2 after blow-down.

## 6. DISCUSSION

In the present article, we have performed a geometric analysis of a singularly perturbed two-variable model for a cyclic AMP (cAMP) signaling system. The model is obtained from a scaling of the three-variable Martiel-Goldbeter model [16] which is due to Liřcanu and Velázquez [15]. The planar system resulting from a quasi-steady-state assumption, Equation (5), represents a two-parameter singular perturbation problem; the presence of two parameters  $\kappa$  and  $\varepsilon$  in the model manifests in a highly degenerate, and non-standard, singular limit as  $(\kappa, \varepsilon) \rightarrow (0, 0)$  which is resolved via a combination of geometric singular perturbation theory and the desingularisation technique known as blow-up. In particular, our approach allows us to describe in detail the global geometry of the model in the limit as both singular perturbation parameters tend to zero; the underlying critical manifold, consisting of one non-hyperbolic line in the “inner” region and one normally hyperbolic curve in the “outer” region which meet at a degenerate equilibrium at the origin, is desingularised in the process. Our resolution of those degeneracies is motivated by a similar study of the Goldbeter-Lefever model by Kosiuk and Szmolyan [13] and permits us to construct a family of periodic (relaxation-type) cycles for Equation (59), thus shedding light on a novel singular perturbation problem and improving our understanding of the corresponding oscillatory dynamics.

In future, we intend to extend our analysis to the three-variable reaction-diffusion system [15]

$$(59a) \quad R_\tau(\tilde{x}, \tau) = \kappa(U + \mathcal{P}\varepsilon) \left[ \frac{\mu(U + \varepsilon) - (U + d\varepsilon)R}{(U + \frac{\varepsilon}{c})(U + \varepsilon)} \right],$$

$$(59b) \quad W_\tau(\tilde{x}, \tau) = \frac{b\varepsilon(U + \varepsilon)^2 + \Theta R^2 U^2}{(U + \varepsilon)^2 + \Lambda R^2 U^2} - W,$$

$$(59c) \quad U_\tau(\tilde{x}, \tau) = U_{\tilde{x}\tilde{x}} + \Gamma(W - U),$$

which incorporates an extracellular cAMP diffusion term, as introduced in [25]. Correspondingly,  $R$ ,  $W$ , and  $U$  are functions of both space  $\tilde{x}$  and time  $\tau$ , with  $x = \sqrt{\frac{D}{k_i + k_t}} \tilde{x}$ ; cf. again Table 1. The main result of [15] is a proof for the existence of traveling pulse solutions to (59) in one spatial dimension on the basis of singular perturbation theory, under the assumption that the parameters  $\kappa$  and  $\varepsilon$  are small; moreover, asymptotic formulae are derived for these pulse solutions in a number of relevant scaling regimes.

We expect that a geometric construction of these solutions can be based on the framework established here, in the context of our simplified two-variable Equation (5). However, in preliminary work, we have not managed to find a scaling for regime  $\mathcal{R}_1$  that allows us to establish an overlap with  $\mathcal{R}_3$ ; recall our discussion in Section 4.4. That failing is mirrored by the fact that a key non-linear eigenvalue problem in [15, Section 4.1.2] has to be solved numerically to allow for the calculation of the unique velocity of travelling pulses. Hence, we believe that further investigation is warranted.

## REFERENCES

- [1] P. Bonckaert, P. De Maesschalck, and F. Dumortier. Well adapted normal linearization in singular perturbation problems. *Journal of Dynamics and Differential Equations*, 23(1):115–139, mar 2011.
- [2] E. Brieskorn and H. Knörrer. *Plane Algebraic Curves: Translated by John Stillwell*. Birkhäuser Verlag Basel, 1986.
- [3] F. Dumortier. Techniques in the theory of local bifurcations: Blow-up, normal forms, nilpotent bifurcations, singular perturbations. In *Bifurcations and Periodic Orbits of Vector Fields*, pages 19–73. Springer Dordrecht, 1993.
- [4] N. Fenichel. Geometric singular perturbation theory for ordinary differential equations. *Journal of Differential Equations*, 31(1):53–98, jan 1979.

- [5] G. Gerisch and B. Hess. Cyclic-AMP-controlled oscillations in suspended dictyostelium cells: Their relation to morphogenetic cell interactions. *Proceedings of the National Academy of Sciences*, 71(5):2118–2122, may 1974.
- [6] G. Gerisch and D. Malchow. Cyclic AMP receptors and the control of cell aggregation in dictyostelium. *Advances in Cyclic Nucleotide Research*, 7:49–68, 1976.
- [7] G. Gerisch, D. Malchow, W. Roos, and U. Wick. Oscillations of cyclic nucleotide concentrations in relation to the excitability of dictyostelium cells. *The Journal of Experimental Biology*, 81:33–47, 1979.
- [8] G. Gerisch and U. Wick. Intracellular oscillations and release of cyclic AMP from dictyostelium cells. *Biochemical and Biophysical Research Communications*, 65(1):364–370, jul 1975.
- [9] A. Goldbeter and L.A. Segel. Unified mechanism for relay and oscillation of cyclic AMP in dictyostelium discoideum. *Proceedings of the National Academy of Sciences*, 74(4):1543–1547, apr 1977.
- [10] A. Goldbeter and L.A. Segel. Control of developmental transitions in the cyclic AMP signalling system of dictyostelium discoideum. *Differentiation*, 17(1-3):127–135, dec 1980.
- [11] G. Hek. Geometric singular perturbation theory in biological practice. *Journal of Mathematical Biology*, 60(3):347–386, 2010.
- [12] C.K.R.T. Jones. *Dynamical Systems: Lectures Given at the 2nd Session of the Centro Internazionale Matematico Estivo held in Montecatini Terme, Italy, June 13–22, 1994*, chapter Geometric singular perturbation theory, pages 44–118. Springer Berlin Heidelberg, 1995.
- [13] I. Kosiuk and P. Szmolyan. Scaling in singular perturbation problems: Blowing up a relaxation oscillator. *SIAM Journal on Applied Dynamical Systems*, 10(4):1307–1343, jan 2011.
- [14] M. Krupa and P. Szmolyan. Extending geometric singular perturbation theory to nonhyperbolic points—fold and canard points in two dimensions. *SIAM Journal on Mathematical Analysis*, 33(2):286–314, jan 2001.
- [15] G. Lițcanu and J.J.L. Velázquez. Singular perturbation analysis of cAMP signalling in dictyostelium discoideum aggregates. *Journal of Mathematical Biology*, 52(5):682–718, mar 2006.
- [16] J.L. Martiel and A. Goldbeter. A model based on receptor desensitization for cyclic AMP signaling in dictyostelium cells. *Biophysical Journal*, 52(5):807–828, nov 1987.
- [17] E.F. Mishchenko and N.Kh. Rozov, *Differential Equations with Small Parameters and Relaxation Oscillations: Translated by F.M.C. Goodspeed*, Plenum Press New York, 1980.
- [18] W. Roos and G. Gerisch. Receptor-mediated adenylate cyclase activation in Dictyostelium discoideum. *FEBS Letters*, 68(2):170–172, oct 1976.
- [19] W. Roos, V. Nanjundiah, D. Malchow, and G. Gerisch. Amplification of cyclic-AMP signals in aggregating cells of Dictyostelium discoideum. *FEBS Letters*, 53(2):139–142, may 1975.
- [20] W. Roos, C. Scheidegger, and G. Gerisch. Adenylate cyclase activity oscillations as signals for cell aggregation in dictyostelium discoideum. *Nature*, 266(5599):259–261, mar 1977.
- [21] L. Segel and A. Goldbeter. Scaling in biochemical kinetics: dissection of a relaxation oscillator. *Journal of Mathematical Biology*, 32(2):147–160, jan 1994.
- [22] B.M. Shaffer. Secretion of cyclic AMP induced by cyclic AMP in the cellular slime mould dictyostelium discoideum. *Nature*, 255(5509):549–552, jun 1975.
- [23] P. Szmolyan and M. Wechselberger. Relaxation oscillations in  $\mathbb{R}^3$ . *Journal of Differential Equations*, 200(1):69–104, jun 2004.
- [24] A. Theibert. Cyclic 3', 5'-AMP relay in dictyostelium discoideum: Adaptation is independent of activation of adenylate cyclase. *The Journal of Cell Biology*, 97(1):173–177, jul 1983.
- [25] J.J. Tyson, K.A. Alexander, V.S. Manoranjan, and J.D. Murray. Spiral waves of cyclic AMP in a model of slime mold aggregation. *Physica D: Nonlinear Phenomena*, 34(1-2):193–207, jan 1989.

UNIVERSITY OF EDINBURGH, SCHOOL OF MATHEMATICS AND MAXWELL INSTITUTE FOR MATHEMATICAL SCIENCES, JAMES CLERK MAXWELL BUILDING, KING'S BUILDINGS, PETER GUTHRIE TAIT ROAD, EDINBURGH EH9 3FD, UNITED KINGDOM

TECHNISCHE UNIVERSITÄT WIEN, INSTITUTE FOR ANALYSIS AND SCIENTIFIC COMPUTING, WIEDNER HAUPTSTRASSE 8-10, 1040 WIEN, AUSTRIA